Phosphorylation-regulated activation of the Arabidopsis RRS1-R/RPS4 immune receptor complex reveals two distinct effector recognition mechanisms

Hailong Guo[1,3], Hee-Kyung Ahn[1,3], Jan Sklenar[1], Jianhua Huang[1], Yan Ma[1,2], Pingtao Ding[1], Frank L.H. Menke[1], and Jonathan D. G. Jones[1,4,*]

[1]The Sainsbury Laboratory, University of East Anglia, Norwich Research Park, Norwich, NR4 7UH, UK

[2]Present address: Department of Plant Molecular Biology (DBMV), Université de Lausanne, 1015 Lausanne, Switzerland

[3]Co-first author

[4]Lead contact

[*]Correspondence: jonathan.jones@tsl.ac.uk (J.D.G.J)

SUMMARY

The Arabidopsis immune receptors RPS4 and RRS1 interact to co-confer responsiveness to bacterial effectors. The RRS1-R allele, with RPS4, recognizes AvrRps4 and PopP2, while RRS1-S responds only to AvrRps4. Here we show that the C-terminus of RRS1-R, but not RRS1-S, is phosphorylated. Phosphorylation at Thr1214 in the WRKY domain maintains RRS1-R in its inactive state, and also inhibits acetylation of RRS1-R by PopP2. PopP2 catalyzes O-acetylation of Thr1214 thereby preventing its phosphorylation. Phosphorylation at the other sites is required for PopP2, but not AvrRps4, responsiveness, and facilitates C-terminal interaction with TIR^{RRS1}. De-repression of RRS1-R or RRS1-S involves effector-triggered proximity between their N-terminal TIR domain and their C-termini. This effector-promoted interaction between TIR^{RRS1} and the RRS1 C-terminus relieves inhibition of TIR^{RPS4} by TIR^{RRS1}. Our data reveal effector-triggered and phosphorylation-regulated conformational changes within RRS1 that results in distinct modes of derepression of the complex by PopP2 and AvrRps4.

INTRODUCTION

Pathogenic microbes have co-evolved with plants for millennia, and can cause devastating crop losses. Plants have evolved a two-layered immune system to defend against pathogen infection (Jones and Dangl, 2006). Cell surface-localized pattern-recognition receptors (PRRs) can directly detect extracellular microbe-derived molecules and initiate immune signaling, activating pattern-triggered immunity (PTI) (Couto and Zipfel, 2016). To circumvent PTI, adapted pathogens secrete a repertoire of effector proteins with a broad range of biochemical functions into plant cells to promote pathogenesis (Wessling et al., 2014). Plants have evolved a repertoire of intracellular nucleotide-binding (NB), leucine-rich repeat (LRR) receptors (NB-LRRs, or NLRs) to sense specific pathogen effectors (Jones et al., 2016). NLRs detect effector proteins either directly or by monitoring effector-mediated modification of host proteins, known as “guardees” or “decoys” (van der Hoorn and Kamoun, 2008). Plant NLRs possess a conserved architecture with a central nucleotide-binding (NB) domain and a C-terminal leucine-rich repeat (LRR) domain (Zhang et al., 2017b), often with an N-terminal Toll/Interleukin-1 receptor/Resistance (TIR) domain or coiled-coil (CC) domain. The specific recognition of pathogen effectors by NLRs leads to activation of effector-triggered immunity (ETI), which includes rapid transcriptional reprogramming and programmed cell death at sites of infection (Maekawa et al., 2011). Despite the central roles of NLRs in plant immunity, the mechanisms of NLR activation and signaling remain largely unknown, though NLR oligomerization upon effector detection has been reported (Wang et al., 2019a; Wang et al., 2019b).

For some NLRs, the C-terminal LRR domain enables direct effector perception. Conformational changes of LRR domains triggered by direct or indirect recognition of effector are thought to allow exchange of ADP for ATP in the central NB-ARC domain, enabling oligomerization of the N-terminal domain (Monteiro and Nishimura, 2018; Takken and Tameling, 2009). For example, the NLR ZAR1 oligomerizes upon activation into a pentamer complex (resistosome), thus imposing induced proximity on its N-terminal CC domains (Wang et al., 2019a; Wang et al., 2019b). Self-association

of TIR domains, including RPP1, L6, RPS4 and SNC1, and CC domains, including MLA10, Sr33, Sr50 and ZAR1, can activate cell death in the absence of pathogen (Bai et al., 2012; Bernoux et al., 2011; Cesari et al., 2016; Krasileva et al., 2010; Zhang et al., 2017a). Mutations of residues in the dimer interface that disrupt self-association also compromise autoactivity.

Several plant NLRs require another NLR for function (Cesari et al., 2014a). In NLR pairs, each NLR specializes as sensor or executor for effector perception and signal initiation, respectively. The sensor NLR can detect effectors via an integrated domain (ID) and often associates with a genetically linked executor NLR, forming immune complexes, such as Arabidopsis RRS1/RPS4, rice RGA4/RGA5 and Pik-1/Pik-2 (Cesari et al., 2014b; Williams et al., 2014; Yuan et al., 2011). Some sensor NLRs require genetically-unlinked NLRs, termed the helpers, to activate signalling (Castel et al., 2018; Peart et al., 2005; Wu et al., 2017). Downstream signalling upon activation of NLRs is still poorly understood. However, for ZAR1, effector-mediated oligomerization of NLR may lead directly to cell death (Wang et al., 2019a; Wang et al., 2019b).

The *Arabidopsis* RRS1-R sensor and RPS4 executor form a complex that responds to two bacterial effectors, PopP2, an acetyl-transferase from *Ralstonia solanacearum* and AvrRps4 from *Pseudomonas syringae* pv. *pisi*. Accessions Nd-1 and Ws-2 carry RRS1-R, but the Col-0 allele of RRS1 (RRS1-S) confers AvrRps4, but not PopP2, recognition. RRS1-R recognizes AvrRps4 and PopP2 via an integrated WRKY domain that mimics the effector's authentic targets (Le Roux et al., 2015; Sarris et al., 2015). The WRKY domain in RRS1 represses receptor activation, and AvrRps4 binding relieves autoinhibitory intramolecular interactions between the WRKY domain (D5) and its adjacent domain 4 (DOM4). PopP2 derepression of RRS1-R/RPS4 requires the longer C-terminal extension of RRS1-R (Ma et al., 2018). However, the mechanism of PopP2 derepression remains unclear. In addition, the role of the C-terminal extension beyond the WRKY domain (D6) in PopP2 responsiveness is poorly understood.

Here we show that the C-terminus of RRS1-R (WRKY domain and C-terminal domain, abbreviated as D56-R), but not RRS1-S (D56-S), is phosphorylated.

Phosphorylation at Thr1214 is required for maintaining RRS1-R in inactive state, and at the other phosphorylation sites in D56-R, for PopP2 but not AvrRps4 responsiveness. We additionally found that Thr1214 phosphorylation inhibits PopP2-mediated acetylation of RRS1-R and PopP2 acetylates Thr1214, thus contributing to RRS1-R activation by leaving Thr1214 incapable of being phosphorylated. De-repression of RRS1 involves effector-triggered enhanced association between the TIR^{RRS1} and C-terminus. Phosphorylation at the other sites of D56-R collectively potentiate its interaction with TIR^{RRS1} and, unlike AvrRps4, PopP2 promotes D56-R association with TIR^{RRS1} in a manner that is dependent on phosphorylation of D56-R. This specific effector-promoted interaction between TIR^{RRS1} and the C-terminus is required to relieve the inhibition of TIR^{RRS1} on TIR^{RPS4}. Taken together, our findings refine our understanding of effector-triggered and phosphorylation-regulated conformational changes within RRS1 that results in distinct modes of derepression of the complex by two different effectors.

RESULTS

The C-terminus of RRS1-R, but not RRS1-S, is phosphorylated *in vivo*.

RRS1-S and RRS1-R differ in the presence of 83 additional amino acids at the RRS1-R C terminus. After transient expression in *Nicotiana benthamiana (Nb),* D56-R migrates as two bands (Fig 1A), in contrast to D56-S (Fig 1B). This slower migrating band disappears after incubation of immunoprecipitated (IP'd) D56-R with λ-phosphatase (Fig 1C), indicating that it contains phosphorylated form(s) of D56-R.

To define its phosphorylated residues, D56-R protein was IP'd from *Arabidopsis* transgenic plants expressing HF-tagged D56-R and subjected to liquid chromatography-tandem mass spectrometry (LC-MS/MS) analysis. We identified multiple phosphorylated residues in D56-R: Ser1203, Thr1214, Ser1296, Ser1315, Ser1316, Ser1317 and/or Thr1318 (the latter four residues could not be precisely differentiated by LC-MS/MS) (Table S1 and Fig S1). No phosphorylated peptides were found in IP'd D56-S. Notably, although Ser1296 and the Ser/Thr cluster(1315-1318) reside in the C-terminal D6 of RRS1-R and are absent in RRS1-S, Ser1203 and

Thr1214 reside in the WRKY domain of both RRS1-R and RRS1-S (Fig 1D), suggesting that protein kinase(s) involved in the phosphorylation of RRS1-R exhibit high specificity. We generated D56-R mutants by replacing each phosphorylated residue with alanine (Ala). For simplicity, we designated these phosphorylated sites with numbers, Ser1203 as 1, Thr1214 as 2, Ser1296 as 3, and the Ser/Thr cluster (1315-1318) together as 4. Simultaneous substitution of all phosphorylated residues led to a complete loss of D56-R mobility shift. Substitution of some but not all residues with Ala results in partial loss of mobility shift. For example, D56-$R^{1/2/3A}$ and D56-R^{4A} show a loss of upper band but still retain some residual mobility shift in the lower band (Fig 1E), suggesting that each Ser and Thr is independently phosphorylated and all phosphorylation sites have an additive effect on the phosphorylation-induced mobility shift.

Phosphorylation at Thr 1214 is required for maintaining RRS1-R in the inactive state, and at other sites, for PopP2 responsiveness

Given that phosphorylation is only detected in RRS1-R, we tested if phosphorylation of RRS1-R is important for PopP2 recognition. We transiently tested RRS1-R mutants for their ability to recognize PopP2 when co-expressed with RPS4 in *N. tabacum* (tobacco) leaves. The non-phosphorylatable mutations of Ser1203 (RRS1-R^{1A}) and Ser/Thr cluster (RRS1-R^{4A}) retain PopP2 recognition, whereas the Ser1296 phosphorylation-deficient RRS1-R (RRS1-R^{S3A}) is slightly impaired in PopP2 recognition (Fig 2A and 2B; cell death scale is shown in Fig S2A). However, the RRS1-$R^{1/3/4A}$ variant carrying all these mutations completely loses responsiveness to PopP2 even though its expression level is similar to wild-type RRS1-R (Fig S2B). These data reveal additive effects of these phosphorylation sites and an essential requirement of D56-R phosphorylation in PopP2-triggered activation. This was further validated by the evidence that in susceptible *Arabidopsis* (Col-0), transgenically expressed RRS1-R but not RRS1-$R^{1/3/4A}$, confers PopP2 recognition and resistance to *P. syringae* expressing PopP2 (Fig 2C and 2D). Intriguingly, the substitution of Thr1214 with Ala (RRS1-R^{2A}) results in constitutive RPS4-dependent autoactivity (Fig 2A). In contrast, the phosphomimic mutant RRS1-R^{2D} loses responsiveness to PopP2 despite similar levels

of protein accumulation (Fig 2E and Fig S2B), indicating that site-specific phosphorylation on RRS1-R exerts distinct effects on its functionality and Thr1214 phosphorylation helps maintain RRS1-R in its inactive form. The remaining RRS1-R single phosphomimic mutants are functional for PopP2 recognition and show no auto-activity, but interestingly, the RRS1-$R^{1/3/4D}$ mutant exhibits auto-activity (Fig 2E and 2F). Phosphorylation-null and phosphomimic mutants of RRS1-R with compromised PopP2 recognition retain AvrRps4 recognition (Fig 2A and 2D), indicating that phosphorylation at D56-R positions 1, 3 and 4 is specifically required for PopP2, but not AvrRps4, recognition.

We also tested whether RRS1-S Thr1212 that corresponds to T1214 in RRS1-R regulates RRS1-S function. Both RRS1-S^{2A} and RRS1-S^{2D} are not autoimmune and induce an AvrRps4-dependent cell death when co-expressed with RPS4 (Fig 2G). These results, together with our previous finding that autoimmunity triggered by RRS1-R^{K1221Q} and RRS1-R^{slh1}(carrying a leucine insertion in WRKY domain), but not by RRS1-S^{K1221Q} and RRS1-S^{slh1} (Noutoshi et al., 2005; Sarris et al., 2015), implies that some of the 83 additional amino acids at the C-terminus of RRS1-R enable this defense activation.

In contrast to other NLRs, RRS1-R is recessive and F1 hybrids resulting from Nd-1/Col-0 or Ws-2/Col-0 crosses lose PopP2 responsiveness. However, Col-0 transgenic lines carrying RRS1-R respond to PopP2 (Deslandes et al., 2002; Williams et al., 2014). RRS1-R^{slh1}-dependent lethality is also recessive in a heterozygote with RRS1-R or RRS1-S. Agroinfiltration of wild-type RRS1 interferes with HR induced by coexpression of RRS1-R^{slh1} and RPS4 (Sohn et al., 2014). We tested if RRS1 interferes with the autoimmunity of RRS1-R^{2A} and RRS1-$R^{1/3/4D}$. Consistent with the recessive nature of RRS1^{slh1}, RRS1-R and RRS1-S prevent constitutive defense activation by RRS1-R^{2A}/RPS4 and RRS1-$R^{1/3/4D}$/RPS4 (Fig S2C), suggesting that autoimmunity of RRS1-R^{2A} and RRS1-$R^{1/3/4D}$ is recessive. Interestingly, simultaneous substitution of all the phosphorylation sites (RRS1-$R^{1/2/3/4A}$) abolishes the autoimmunity of RRS1-R^{2A} but still retains AvrRps4 but not PopP2 responsiveness (Fig S2D), suggesting that autoimmunity of RRS1-R^{2A} requires phosphorylation of D56-R at the rest of

phosphorylation sites *in cis.* In agreement with the transient assay, introducing RRS1-R^{2A} into *Arabidopsis* Col-0 background leads to severe stunting and necrotic lesions, whereas transgenic plants containing RRS1-$R^{1/2/3/4A}$ show a wild-type phenotype (Fig S2E). Autoimmunity of RRS1-R^{slh1} and RRS1-R^{K1221Q} also requires phosphorylation of D56-R at the positions 1, 3 and 4, since the autoimmunity of RRS1-R^{slh1} and RRS1-R^{K1221Q} is also suppressed by simultaneous introduction of these mutations *in cis* (Fig S2F).

Antagonistic interplay between Thr1214 phosphorylation and acetylation of WRKY domain regulates RRS1-R function

The RRS1-$R^{1/3/4A}$ variant loses responsiveness to PopP2 but not to AvrRps4. RRS1-R/RPS4-mediated defense activation by PopP2 requires PopP2-dependent acetylation of RRS1-R WRKY motif, in particular, K1217 and K1221 (Le Roux et al., 2015; Sarris et al., 2015). The lack of PopP2 responsiveness in RRS1-$R^{1/3/4A}$ possibly results from loss of interaction with PopP2 or the ability to be acetylated by PopP2. Since PopP2 still interacts with RRS1-$R^{1/3/4A}$ (Fig S3A), we tested whether the C-terminal phosphorylation of RRS1-R is required for acetylation. We co-expressed wild-type RRS1-R and non-phosphorylatable forms of RRS1-R with PopP2 in the absence of RPS4 in *Nb* leaves. RRS1 proteins were IP'd and their acetylation by PopP2 was determined by immunoblotting with anti-acetyl-lysine antibody (α-Ac-K). RRS1-$R^{1/3/4A}$ was acetylated to a similar level as the wild-type RRS1-R (Fig 3A). Therefore, the loss of PopP2 responsiveness is not due to loss of acetylatability by PopP2, indicating that RRS1-R does not need to be phosphorylated for acetylation to occur, consistent with PopP2 acetylation of the C-terminus of RRS1-S (Sarris et al., 2015). Interestingly, mutation of Thr1214 either alone (RRS1-R^{2A}) or in combination with the rest of phosphorylation sites (RRS1-$R^{1/2/3/4A}$) increased RRS1-R acetylation, whereas acetylation is severely reduced in the phosphomimic RRS1-R^{2D} (Fig 3A), which may contribute to its compromised PopP2 responsiveness. We used selected reaction monitoring (SRM) to quantify the relative level of double-lysine-acetylation peptides of WRKY motif by PopP2. These data further confirmed that double-lysine-acetylation is increased in RRS1-R^{2A} but largely decreased in the RRS1-R^{2D} (Figure 3B). Since

Thr1214 is in close proximity to the two lysine residues of WRKY domain, we speculate that phosphorylation of Thr1214 antagonizes neighboring lysine acetylation during RRS1 activation. Acetylation was not decreased in other RRS1-R phosphomimic mutants (Fig S3B), consistent with an inhibitory role of phosphorylation on RRS1-R activity specified by the Thr1214.

PopP2 belongs to the YopJ family of acetyltransferases such as HopZ1a and HopZ3, which can also acetylate serine and threonine residues (Mukherjee et al., 2006; Lewis et al., 2013; Ma and Ma, 2016). Similarly, in addition to the previously identified lysine residues in the WRKY domain, we found that PopP2 also acetylates RRS1-R at Thr1214 (Fig S3C), indicating that acetylation directly competes with phosphorylation of the same threonine. Conceivably, owing to the dynamic phosphorylation and dephosphorylation *in vivo*, PopP2-mediated O-acetylation of the hydroxyl group in unphosphorylated Thr1214 leaves it incapable of accepting phosphates (being phosphorylated), also promoting RRS1-R activation.

To examine whether phosphorylation and acetylation mutually affect each other, we introduced the phosphomimic T1214D into acetyl-mimic background (RRS1-R^{K1221Q}) and found that mimicking phosphorylation of Thr1214 dampens the autoimmunity of RRS1-R^{K1221Q} (Fig 3C), indicating that autoimmunity triggered by mimicry of K1221 acetylation requires T1214 to be dephosphorylated. The phosphomimic T1214D cannot be "dephosphorylated", thus inhibiting the autoactivity of RRS1-R^{K1221Q}. Conversely, autoimmunity of RRS1-R^{2A} is also inhibited by introducing the non-acetylatable mutation (RRS1-R^{K1221R}) although all mutant proteins expressed at similar levels (Fig 3D and Fig S3D), suggesting that low levels of PopP2-independent basal acetylation of K1221 might be required for the autoactivity of RRS1-R^{2A}. These data again imply that Thr1214 phosphorylation keeps RRS1-R in its inactive state and acetylation of K1221 is needed to switch to an activated state. Phosphorylation of T1214 and acetylation of K1221 thus play a mutually antagonistic role in RRS1-R activation.

RRS1-S C-terminus interacts with its TIR domain in an AvrRps4-dependent manner, and RRS1-R C-terminus association with its TIR domain is enhanced by AvrRps4 and PopP2

As C-terminal phosphorylation of RRS1-R is not required for PopP2-mediated acetylation, we tested whether phosphorylation modulates RRS1-R intramolecular reconfiguration and PopP2-dependent activation using bimolecular fluorescence complementation (BiFC) assay. The N-terminal half of the yellow fluorescent protein (nVenus) was fused to the C- terminus of RRS1-S, and the C-terminal half of CFP was fused to its N-terminus. RRS1 with N- and C- terminal fusion tags confers responsiveness to AvrRps4 when co-expressed with RPS4, though weaker than wild-type RRS1 (Fig S4A and S4B). In the absence of effector, no signal was detected, but interestingly, BiFC signal of cCFP:RRS1-S:nVenus was observed in the presence of AvrRps4, but not with AvrRps4^{EEAA} (EEAA) or PopP2 (Fig 4A). Lack of YFP signal is not due to the lack of protein expression (Fig S4C), indicating that AvrRps4 enables the BiFC signal of N- and C-terminal fluorescent-tagged RRS1-S. We concluded that RRS1-S TIR and C-terminus become in closer proximity upon AvrRps4 perception. To further examine whether AvrRps4 could enable the interaction between TIR^{RRS1} and C-terminus, we performed co-immunoprecipitation (Co-IP) assay after transient coexpression of TIR^{RRS1} and D56-S in *Nb* leaves. TIR^{RRS1} and D56-S association is only detected in the presence of AvrRps4, but not of EEAA or PopP2 (Fig 4B), confirming that AvrRps4 promotes a specific interaction between TIR^{RRS1} and D56-S. This idea is further supported by the BiFC experiment by coexpressing separate TIR^{RRS1} and D56-S fused to the split fluorophore fragments (Fig S4D). Thus, failure to induce TIR^{RRS1} and D56-S association by PopP2 correlates with the lack of defense activation of RRS1-S/RPS4 by PopP2.

We tested the association between TIR^{RRS1} and D56-R upon effector recognition. In contrast to RRS1-S, YFP signal was observed when RRS1-R was N-terminally tagged with cCFP and C-terminally tagged with nVenus in both presence and absence of effectors (Fig 4C), indicating that the longer D56-R enables a constitutive BiFC signal with TIR^{RRS1}. We further confirmed the interaction between TIR^{RRS1} and D56-R using

Co-IP. FLAG-tagged D56-R co-IP'd with GFP-tagged TIR^{RRS1}, but not with GFP alone (Fig 4D and S4E). Since the WRKY domain of RRS1-R is almost identical to that of RRS1-S, the observed TIR^{RRS1} interaction difference between D56-R and D56-S is likely due to the 83 aa C-terminal extension, suggesting that some of these amino acids contribute to the D56-R interaction with TIR^{RRS1}. Notably, the C-terminal extension is predicted to be intrinsically disordered (Fig S4F). Intrinsically disordered regions (IDRs) generally serve as flexible linkers/spacers in multi-domain proteins or between structured domains (Meng and Kurgan, 2016; van der Lee et al., 2014). Thus, the constitutive TIR^{RRS1}/D56-R association could be explained by the flexible region that connects the structured TIR and WRKY domain.

We next examined this interaction in the presence of effectors. Intriguingly, the association between TIR^{RRS1} and D56-R is enhanced in the samples coexpressing AvrRps4 and PopP2 but not effector mutants (Fig 4D). Taken together, these results imply that the TIR^{RRS1} contributes to de-repression, and that de-repression of RRS1 involves effector-triggered proximity or enhancement of affinity between TIR^{RRS1} and the RRS1 C-terminus. AvrRps4 promotes interaction of TIR^{RRS1} with C-terminus of RRS1-R and RRS1-S, but PopP2 only promotes interaction of TIR^{RRS1} with C-terminus of RRS1-R, consistent with RRS1-R responsiveness to PopP2 and AvrRps4, whereas RRS1-S responds only to AvrRps4.

Phosphorylation of D56-R potentiates its interaction with TIR^{RRS1} and is required for PopP2-, but not AvrRps4-, promoted interaction with TIR^{RRS1}.

The involvement of effector-enhanced TIR^{RRS1}/C-terminus proximity in RRS1 de-repression led us to examine whether D56-R phosphorylation influences its effector-dependent association with TIR^{RRS1}. Protein extracts prepared from *Nb* leaves expressing D56-R protein were dephosphorylated with λ-phosphatase and then used for Co-IP assay. Dephosphorylation of D56-R significantly reduced its affinity for TIR^{RRS1} (Fig 5A), indicating that phosphorylation of D56-R promotes its binding to TIR^{RRS1}. We next generated D56-$R^{1/3/4A}$ and found its association with TIR^{RRS1} is strongly reduced, though not abolished (Fig 5B). To substantiate these data, phosphomimic D56-$R^{1/3/4D}$ variant was tested for its ability to interact with TIR^{RRS1}

because some phosphorylated forms of D56-R migrate with unphosphorylated D56-R (Fig S5A). D56-$R^{1/3/4D}$ enhanced its interaction with TIR^{RRS1} (Fig 5C) and this constitutive interaction is insensitive to λ-phosphatase (Fig S5B), confirming phosphorylation enhances its interaction with TIR^{RRS1}.

Since effector-promoted interaction of TIR^{RRS1} with the C-terminus of RRS1 is involved in RRS1/RPS4 activation, we tested if effectors influence interactions of D56-R or D56-$R^{1/3/4A}$ with TIR^{RRS1}. Like wild-type D56-R, D56-$R^{1/3/4A}$ association with TIR^{RRS1} is greatly enhanced in the presence of AvrRps4 (Fig 5D), implying that AvrRps4 can promote both wild-type D56-R and non-phosphorylatable D56-$R^{1/3/4A}$ association with TIR^{RRS1}. However, PopP2 only promotes TIR^{RRS1}/D56-R but fails to enhance TIR^{RRS1}/D56-$R^{1/3/4/A}$ interaction (Fig 5D), indicating that phosphorylation at these sites is essential for the enhanced TIR^{RRS1}/D56-R association upon PopP2 perception. Likewise, this enhancement of TIR^{RRS1}/D56-R association by PopP2, but not AvrRps4, was abolished when pretreated with λ-phosphatase (Fig S5C). Thus, failure to promote TIR^{RRS1} and D56-$R^{1/3/4A}$ association by PopP2 could explain why it fails to activate RRS1-$R^{1/3/4A}$/RPS4.

The observation that AvrRps4 can enhance the association of TIR^{RRS1} with D56-R, D56-$R^{1/3/4A}$ and D56-S led us to hypothesize that AvrRps4 may be able to associate with TIR^{RRS1}, thus functioning as a ”molecular glue” by promoting RRS1 intramolecular interaction. We found that AvrRps4, but not EEAA and PopP2, co-IPs with TIR^{RRS1} (Fig S5D), consistent with our previous finding that AvrRps4, but not PopP2, still co-IPs with RRS1 WRKY/LexA in which the WRKY domain was replaced with the bacterial LexA domain (Sarris et al., 2015). Since AvrRps4 can associate with TIR^{RRS1} and WRKY domain, it could promote TIR^{RRS1} association with D56-R, D56-$R^{1/3/4A}$ and D56-S, independent of phosphorylation because D56-S is not phosphorylated. PopP2 does not associate with TIR^{RRS1}, and therefore only enhances proximity of TIR and D56-R in RRS1-R in a phosphorylation-dependent manner.

Effector-promoted interaction between TIR^{RRS1} and C-terminus releases the inhibition of TIR^{RRS1} on TIR^{RPS4}

How effector sensing via RRS1 WRKY domain leads to signaling activation via TIR^{RPS4} is still unclear. TIR^{RPS4}-triggered cell death can be suppressed by coexpression with TIR^{RRS1}, likely due to higher affinity of TIR^{RRS1}/TIR^{RPS4} heterodimerization suppressing homodimerization of TIR^{RPS4} (Williams et al., 2014). Conceivably, effector-enhanced N- and C-terminal association of RRS1 releases TIR^{RPS4} from TIR^{RRS1}, enabling homodimerization of TIR^{RPS4} and immune signaling. Therefore, we performed BiFC analysis to test if proximity between TIR^{RRS1} and TIR^{RPS4} is perturbed by effectors. We fused the N-terminal fragment of YFP to the N-terminus of RRS1 (nYFP-RRS1-HF), and the C-terminal fragment of YFP to the N-terminus of RPS4 (cYFP-RPS4-HF). Both proteins were also fused with HF tag at their C-termini to monitor protein levels. The functionality of nYFP-RRS1-R-HF and cYFP-RPS4-HF were confirmed by its responsiveness to AvrRps4 and PopP2, although the responsiveness is weaker than wild-type RRS1 and RPS4 (Fig S6A, B).

YFP signal was observed when nYFP-RRS1-R-HF and cYFP-RPS4-HF were coexpressed. However, the YFP signal was reduced in the presence of AvrRps4 and PopP2, but not by effector mutants EEAA and $PopP2^{C321A}$ (C321A) (Fig 6A, B). Protein accumulation of nYFP-RRS1-R-HF and cYFP-RPS4-HF was slightly reduced in AvrRps4 coexpressed samples, but PopP2 coexpressed samples showed stronger protein accumulation, indicating reduced signal is not explained by protein accumulation (Fig S6C).The BiFC signal of nYFP-RRS1-S-HF and cYFP-RPS4-HF was also significantly reduced when expressed with AvrRps4. However, the YFP signal was only slightly reduced by PopP2, and the interference of YFP intensity by PopP2 was indistinguishable from C321A (Fig 6C, D, and Fig S6D). Collectively, these data imply that the enhancement of affinity between TIR^{RRS1} and the C-terminus of RRS1 by AvrRps4 correlates with a reduced TIR^{RRS1}/TIR^{RPS4} BiFC signal in both RRS1-R and RRS1-S. However, PopP2 perception only suppresses the TIR^{RRS1}/TIR^{RPS4} BiFC signal in RRS1-R, but not RRS1-S, consistent with the failure of PopP2 to enhance the association between N- and C- termini in RRS1-S.

Finally, we investigated how the TIR^{RRS1}/TIR^{RPS4} BiFC signal produced by $RRS1\text{-}R^{1/3/4A}$ and RPS4 changes in the presence of effectors. Coexpression with AvrRps4 but

not EEAA reduced the YFP signal of nYFP-RRS1-$R^{1/3/4A}$-HF and cYFP-RPS4-HF, which is similar to RRS1-R. Although PopP2 also exhibits slight interference of YFP signal, the interference by PopP2 is similar to C321A (Fig 6E, F and Fig S6E), consistent with the inability of RRS1-$R^{1/3/4A}$ to recognize PopP2. Therefore, we conclude that the effector perception by RRS1 C-terminus enhances its affinity to TIR^{RRS1} and subsequently leads to less proximity of TIR^{RRS1} and TIR^{RPS4}, thus enabling formation of a signaling-competent TIR^{RPS4} although RRS1 still associates with RPS4 in post-activation state (Huh et al., 2017).

DISCUSSION

In NLRs, the transition from the resting state to the active state involves intricate inter- and intramolecular reconfigurations. The RRS1/RPS4 NLR pair provides a useful model for molecular understanding of paired NLR protein mechanisms. These findings and previous work reveal that effector recognition triggers at least three conformational rearrangements that convert effector sensing via the RRS1 WRKY domain to signaling activation via the RPS4 TIR domain. We propose that effector binding to the WRKY domain reduces its affinity for DOM4 and concomitantly enhances its interaction with TIR^{RRS1}, reducing proximity between TIR^{RRS1} and TIR^{RPS4}, abrogating the negative regulation of TIR^{RRS1} on TIR^{RPS4}, and eventually enabling TIR^{RPS4} to self-associate.

AvrRps4 and PopP2 enhance TIR^{RRS1} association with C-terminus in a recognition-specific manner and the enhanced association is required for de-repression

Our biochemical and cell biology data suggest effector-enhanced interactions between RRS1 N- and C-termini comprise a critical reconfiguration step involved in derepression of the RRS1/RPS4 complex. In the RRS1-S/RPS4 preactivation state, TIR^{RRS1} and D56-S are not in close proximity, and AvrRps4, but not PopP2, enables TIR^{RRS1}/D56-S interaction. In contrast to RRS1-S, in RRS1-R the longer C-terminal intrinsically disordered region can extend to TIR^{RRS1} in the pre-activation state. D56-R affinity for TIR^{RRS1} is enhanced by both AvrRps4 and PopP2, but not by non-recognized effector mutants. Thus, the enhanced association between TIR^{RRS1} and its C-terminus

promoted by recognized effectors correlates with their ability to derepress the complex, suggesting that effector-dependent enhanced interaction of TIR^{RRS1} with the C-terminus is crucial for immune receptor activation. In addition, our data collectively demonstrate that the ability to promote TIR^{RRS1} and D56-S association distinguishes AvrRps4 and PopP2 responsiveness. The inability to promote TIR^{RRS1}/D56-S association by PopP2 could explain why the RRS1-S only responds to AvrRps4.

Our data suggest that upon effector-enhanced N- and C-terminal proximity of RRS1, release of TIR^{RPS4} from its interaction with TIR^{RRS1} converts effector-induced changes at its C-terminus into signal initiation. TIR^{RPS4} triggers effector-independent cell death when overexpressed and co-expression of TIR^{RRS1} suppresses its autoactivity (Williams et al., 2014), likely due to high affinity between the TIR^{RRS1}/TIR^{RPS4} heterodimer through the AE interface suppressing TIR^{RPS4} self-association mediated by both AE and DE interfaces (Zhang et al., 2017). We propose that effector-enhanced TIR^{RRS1} association with the C-terminus may free TIR^{RPS4} from the TIR^{RRS1}/TIR^{RPS4} heterodimer, enabling it to initiate immune signaling. In support of this, the ability of AvrRps4 and PopP2 to suppress the BiFC signal produced by TIR^{RRS1}/TIR^{RPS4} proximity correlates with their ability to enhance the interaction between TIR^{RRS1} with allele-specific C-terminus. Thus, TIR^{RPS4} inhibited in the resting state by TIR^{RRS1} may become available for self-association–dependent NAD^+-hydrolysis activity associated with cell death signaling. Notably, RPS4, but not RRS1, has the catalytic glutamate for NADase activity in its TIR (Horsefield et al., 2019; Wan et al., 2019). Similarly, in singleton NLRs such as L6 and RPP1, the TIR autoactive signaling triggered by homodimerization is intramolecularly inhibited by their NB-ARC domains in the preactivation state (Bernoux et al., 2011; Schreiber et al., 2016), although it is unclear how the NB-ARC releases its negative regulatory effect on TIR upon effector recognition by the LRR.

Phosphorylation/dephosphorylation adds another layer of complexity to the molecular dynamics that accompany NLR activation

The integrated WRKY domain not only functions as an effector sensor but also plays a pivotal role in the regulation of the immune complex. Mutation, acetylation, or deletion

of the WRKY domain leads to autoactivity (Ma et al., 2018; Noutoshi et al., 2005; Sarris et al., 2015). Here, we reveal another layer of complexity to the regulation of the complex by demonstrating that the WRKY domain and adjacent amino acids are phosphorylated by unknown protein kinase(s) and distinct phosphorylation sites play differential roles in the regulation of RRS1-R function. Compared to PTI, which largely relies on phosphorylation dynamics to activate defense (Mithoe and Menke, 2018), phosphorylation events during ETI are under-investigated. Most importantly, our findings provide, for the first time, an example of plant NLR autoinhibition and functionality regulated by phosphorylation.

Phosphorylation of Thr1214 within the WRKY domain is required to keep RRS1-R in the autoinhibited state and dephosphorylation might release autoinhibition, leading to defense activation. Thr1214 is also a target for O-acetylation by PopP2, so acetylation of Thr1214 might antagonize phosphorylation, thus contributing to RRS1 derepression. Similarly, inflammasome sensor Pyrin is autoinhibited by phosphorylation via phosphorylation-dependent interaction with 14-3-3 proteins and undergoes dephosphorylation upon infection, leading to 14-3-3 dissociation and Pyrin inflammasome assembly (Park et al., 2016). No phosphorylation was observed in the C-terminus of RRS1-S. We propose that the C-terminal 83 aa IDR functions as kinase-docking domain. Indeed, previous studies demonstrated that kinase docking sites are enriched within IDRs and occurrence of post-translational modification including phosphorylation is more frequently observed within IDRs than structured regions (Bah and Forman-Kay, 2016; Collins et al., 2008; Tyanova et al., 2013), implying the general importance of IDRs for signaling and regulation. Further identification of the kinase(s)/phosphatase(s) involved will be an important step towards understanding the regulation of RRS1-R functionality through dynamic cycles of phosphorylation and dephosphorylation.

Phosphorylation at positions 1, 3 and 4 is essential for PopP2 recognition and RRS1-$R^{1/3/4D}$ is autoactive, consistent with the stronger TIR^{RRS1} association with D56-$R^{1/3/4D}$ but not D56-$R^{1/3/4A}$. Since *in vivo* there is a mix of RRS1-R phosphorylation states, and RRS1-R is recessive, non-activated RRS1-R forms attenuate constitutively active

phosphorylated forms. Phosphorylation of the C-terminal IDR might affect its flexibility and enhance subsequent interactions with TIR^{RRS1}. Similarly, RIN4 is an intrinsically disordered protein and RIN4 phosphorylation mimics exhibited enhanced flexibility and stronger interaction with plasma membrane H^+-ATPase AHA1 (Lee et al., 2015). Unlike AvrRps4 which can interact with both the WRKY and TIR^{RRS1} to strengthen their interaction, PopP2-enhanced association requires phosphorylation of D56-R at these residues, implying that phosphorylation combined with PopP2 acetylation of WRKY enables this conformational rearrangement. This is further supported by the lack of decrease in proximity between TIR of RRS1-$R^{1/3/4A}$ and TIR^{RPS4} in the presence of PopP2. While these experiments supported an important role of phosphorylation in the regulation of PopP2-promoted TIR^{RRS1}/D56-R interaction, the possibility that these phosphorylation site substitutions might cause other changes than phosphorylation cannot be excluded. Additionally, the mutually inhibitory interplay between acetylation and phosphorylation of RRS1-R discovered in this study reveals that complex posttranslational regulation works in a coordinated fashion to regulate the activity of RRS1-R.

In marked contrast, phosphorylation is dispensable for AvrRps4 recognition, consistent with the absence of phosphorylation in the C-terminus of RRS1-S. C-terminal phosphorylation is specifically essential for RRS1-R PopP2 responsiveness, verifying again that AvrRps4 and PopP2 have different modes of action to derepress the complex (Ma et al., 2018). These findings, combined with our previous report that PopP2 and AvrRps4 responsiveness involve distinct genetic requirements in RRS1 and RPS4, not only provide fundamental mechanistic insights into how a single sensor NLR operates to recognize different effectors, but also have broad implications for the mechanistic studies of pathogen recognition and activation for other plant NLR pairs.

ACKNOWLEDGMENTS

We thank the Gatsby Foundation (UK) for funding to the Jones lab. We highly appreciate comments from anonymous reviewers which helped us significantly to improve the manuscript. We gratefully acknowledge former lab members, especially Dr. Kee Hoon Sohn, Dr. Sung Un Huh, and Dr. Panagiotis F. Sarris for previous work

that provided important background information for this research report. The authors thank Mark Youles in TSL Synbio for his excellent support with Golden Gate cloning and for providing modules. H.G. and H.A. were supported by ERC Advanced Grant "ImmunitybyPairDesign"; Y.M. was supported by Biotechnology and Biological Sciences Research Council (BBSRC) grant BB/M008193/1. P.D. was supported by European Union's Horizon 2020 research and innovation program under the Marie Skłodowska-Curie Actions (grant 656243).

AUTHOR CONTRIBUTIONS

Conceptualization, H.G., H.A., F.M., J.D.G.J.; Investigation, H.G., H.A., J.S., J.H. and Y.M.; Writing – Original Draft, H.G., H.A., J.D.G.J.; Writing – Review & Editing, H.G., H.A., J.D.G.J.; Funding Acquisition, J.D.G.J.; Resources, P.D.; Supervision, J.D.G.J.

DECLARATION OF INTERESTS

The authors declare no competing interests.

FIGURE LEGENDS

Figure 1. C-terminus of RRS1-R, but not RRS1-S, is phosphorylated *in vivo*.

(A) D56-R migrates as two bands independently of effectors. Total protein was extracted from *Nb* leaves transiently co-expressing D56-R-HF with mCherry (mCh), AvrRps4:mCh and PopP2:mCh at 2 dpi and then subjected to immunoblotting.

(B) D56-R, but not D56-S, migrates as two bands. Total protein was extracted from 4-week-old *Arabidopsis* transgenic plants expressing D56-R-HF and D56-S-HF and then subjected to immunoblotting.

(C) Characterization of up-shifted band of D56-R by dephosphorylation. IP'd D56-R protein from 4-week-old *Arabidopsis* transgenic expressing D56-R-HF were incubated with (+) or without (-) λ-phosphatase (λ-PPase) and then subjected to immunoblotting.

(D) Schematic diagram of domain structures and sequence alignment of the WRKY domain (W, D5) and D6 of RRS1-R/RRS1-S. The WRKY motif is highlighted in red, and the identified phosphorylation sites are marked with black triangles. Two major

PopP2-dependent acetylated lysines in the WRKY domain are marked with black asterisks. Amino acids of D5 and D6 are indicated in gray and yellow, respectively.

(E) Additive effect of phosphorylation site mutations within D56-R on its mobility shift. Total protein was extracted from *Nb* leaves transiently expressing indicated constructs at 2 dpi and then subjected to immunoblotting.

Ponceau S staining was used to demonstrate equal loading. See also **Figure S1**.

Figure 2. Phosphorylation at Thr 1214 is required for maintaining RRS1-R in the inactive state, and at the other sites, for PopP2 responsiveness.

(A) Assessing functionality of non-phosphorylatable RRS1-R in response to AvrRps4 and PopP2. Each tobacco leaf section was transiently infiltrated with RPS4 and indicated constructs, together with either mCherry, AvrRps4 or PopP2.

(C) PopP2-triggered HR in the transgenic *Arabidopsis* (Col-0) line carrying RRS1-R but not RRS1-$R^{1/3/4A}$. PopP2 was delivered from *P. fluorescens* strain Pf0-1 into leaves of 5-week-old *Arabidopsis* plants.

(D) Transgenically expressed RRS1-$R^{1/3/4A}$ does not confer resistance to *Pto* DC3000 (PopP2). PopP2 and C321A were delivered from *P. syringae pv. tomato* DC3000 and bacterial colonies were quantified at 3 dpi.

(E) Impact of phosphomimic mutations on AvrRps4 and PopP2 responsiveness in RRS1-R. Each tobacco leaf section was transiently infiltrated with RPS4 and indicated constructs together with either mCherry, AvrRps4 or PopP2.

(B and F) Percentage representations of cell death scales in **(A)** and **(E)** at 3 dpi. Stacked bars are color-coded to show the proportions (in percentage) of each cell death scale (0–5) out of total infiltrated leaves scored. Total of 12-14 leaves are scored for each stacked column.

(G) Impact of non-phosphorylatable and phosphomimic mutations of T1212 on AvrRps4 responsiveness in RRS1-S. Each tobacco leaf section was transiently infiltrated with RPS4 and indicated constructs together with mCherry or AvrRps4. HRs were assessed at 3 dpi. Phenotypes are representative of at least three consistent replicates. See also **Figure S2**.

Figure 3. Antagonistic interplay between Thr1214 phosphorylation and acetylation of WRKY domain regulates RRS1-R activity.

(A) Effect of mutations of phosphorylation sites on RRS1-R acetylation status. IP'd RRS1-R proteins from *Nb* leaves transiently expressing indicated constructs with mCherry or PopP2 without RPS4 at 2 dpi and then subjected to immunoblotting with α-FLAG antibody for detecting RRS1-R or α-Ac-K antibody for detecting acetylated RRS1-R.

(B) Relative levels of the double-lysine-acetylated KYGQKDILGSR peptides in the WRKY motif of RRS1-R phosphorylation site mutants indicated in **(A)** determined by SRM. Data are represented as means±SD(n=3). n.d., not detected.

(C) Mutually antagonistic interplay between phosphorylation and acetylation in regulating RRS1-R activity. Each tobacco leaf section was transiently infiltrated with RPS4 and indicated constructs.

(D) Percentage representations of cell death scales in **(C)** at 3 dpi. Stacked bars are color-coded to show the proportions (in percentage) of each cell death scale (0–5) out of the total infiltrated panels scored. Total of 13-17 leaves are scored for each stacked column.

See also **Figure S3**.

Figure 4. RRS1-S C-terminus interacts with its TIR domain in an AvrRps4-dependent manner, and RRS1-R C-terminus association with its TIR domain is enhanced by AvrRps4 and PopP2.

(A) BiFC assays reveal N- and C-terminal proximity of RRS1-S upon AvrRps4 perception. The cCFP-RRS1-S-nVenus and AvrRps4:mCh were transiently co-expressed in *Nb* leaves and YFP fluorescence was visualized at 2 dpi. Controls include mCh, AvrRps4 mutant EEAA(EEAA:mCh), PopP2:mCh and PopP2 mutant C321A (C321A:mCh). Scale bar, 5μm.

(B) Co-IP assays for the interaction of TIR^{RRS1} with D56-S in the presence of AvrRps4. Total extracts from *Nb* leaves transiently expressing TIR^{RRS1}-GFP and D56-S-HF at 2 dpi were IP'd with α-GFP beads followed by immunoblotting. Controls include mCh, EEAA:mCh, PopP2:mCh and C321A:mCh.

(C) BiFC assays reveal constitutive N- and C-terminal proximity of RRS1-R. The cCFP-RRS1-R-nVenus was transiently co-expressed with mCh, AvrRps4:mCh, EEAA:mCh, PopP2:mCh and C321A:mCh in *Nb* leaves. The YFP signal is observed at 2 dpi. Scale bar, 5 μm.

(D) Co-IP assays for the interaction of TIR^{RRS1} with D56-R influenced by effectors. Samples were harvested from *Nb* leaves transiently co-expressing TIR^{RRS1}-GFP and D56-R-HF together with mCh, AvrRps4:mCh, EEAA:mCh, PopP2:mCh and C321A:mCh at 2 dpi. Total extracts were IP'd with α-GFP beads followed by immunoblotting. Relative D56-R band intensity is denoted below (Co-IP products normalized to the amounts of Input and relative to control).

All the experiments were repeated three times with similar results. See also **Figure S4**.

Figure 5. Phosphorylation of D56-R potentiates the interaction with TIR^{RRS1} and is required for PopP2-, but not AvrRps4-, promoted interaction with TIR^{RRS1}.

(A) Effect of phosphorylation on TIR^{RRS1}/D56-R interaction. Total protein extracts from *Nb* leaves expressing D56-R-HF and TIR^{RRS1}-GFP were either incubated with buffer alone (-) or with λ-PPase (+) for 30 min at 30°C.The mixture was then IP'd with α-GFP or α-FLAG beads followed by immunoblotting.

(B) The mutation of phosphorylation sites reduces TIR^{RRS1} interaction with D56-R. Samples were harvested from *Nb* leaves transiently co-expressing TIR^{RRS1}-GFP and indicated constructs at 2 dpi. Total extracts were IP'd with α-GFP beads followed by immunoblotting.

(C) Analysis of the interactions between D56-R, D56-$R^{1/3/4A}$, D56-$R^{1/3/4D}$, and TIR^{RRS1}. Total extracts from *Nb* leaves transiently expressing indicated constructs combinations at 2 dpi were IP'd with α-GFP beads followed by immunoblotting.

(D) PopP2, but not AvrRps4, fails to promote the D56-$R^{1/3/4A}$ association with TIR^{RRS1}. Total extracts from *Nb* leaves transiently co-expressing TIR^{RRS1}-GFP and D56-$R^{1/3/4A}$-HF together with mCh, AvrRps4:mCh and PopP2:mCh at 2dpi were IP'd with α-GFP beads followed by immunoblotting.

All the experiments were repeated three times with similar results. Numbers denoted below indicate relative D56-R band intensity (Co-IP products normalized to the amounts of Input and relative to control). See also **Figure S5**.

Figure 6. Effector-promoted interaction between TIR^{RRS1} and C-terminus releases the inhibition of TIR^{RRS1} on the TIR^{RPS4}.

(A) BiFC assays reveal a decrease in proximity between $TIR^{RRS1\text{-}R}$/TIR^{RPS4} upon coexpression with AvrRps4 and PopP2.

(C) BiFC assays reveal a decrease in proximity between $TIR^{RRS1\text{-}S}$/TIR^{RPS4} upon coexpression with AvrRps4 but not PopP2.

(E) BiFC assays reveal a decrease in proximity between $TIR^{RRS1\text{-}R1/3/4A}$/$TIR^{RPS4}$ upon coexpression with AvrRps4 but not PopP2.

nYFP-RRS1-R-HF **(A)**, nYFP-RRS1-S-HF **(C)**, and nYFP-$RRS1\text{-}R^{1/3/4A}$-HF **(E)** constructs are expressed with cYFP-RPS4-HF for YFP reconstitution. mCh, AvrRps4:mCh, EEAA:mCh, PopP2:mCh, and C321A:mCh were coexpressed in *Nb* leaves. CFP was also coexpressed in each experiment as internal control and fluorescence was visualized at 2dpi. Scale bar, 5μm.

(B), (D), (F) Quantification of YFP intensity in **(A)**, **(C)**, and **(E)**, respectively, normalized to the intensity of CFP of individual nuclei. Nuclei from 10 cells were counted for each biological replicate, and individual biological replicates were plotted with different colors. Different letters above the data points indicate significant differences ($P<0.05$).See also **Figure S6**.

STAR★METHODS

Detailed methods are provided in the online version of this paper and include the following:

- KEY RESOURCES TABLE
- CONTACT FOR REAGENT AND RESOURCE SHARING
- EXPERIMENTAL MODEL AND SUBJECT DETAILS

- *Arabidopsis*
- *Nicotiana benthamiana*
- Bacterial Strains

- METHOD DETAILS
  - Plasmid Construction
  - Agrobacterium-Mediated Tobacco Transient Assays (HR)
  - HR Assay in *Arabidopsis*
  - Disease Resistance Assay
  - Protein Extraction, Immunoprecipitation and Immunoblot Analysis
  - Bimolecular Fluorescence Complementation (BiFC) Assay
  - Sample Preparation for Mass Spectrometry
  - LC-MS/MS Analysis
  - Acetylated Peptides Quantitative Assay
  - Software Processing and Peptides Identification
- QUANTIFICATION AND STATISTICAL ANALYSIS

REFERENCES

Bai, S., Liu, J., Chang, C., Zhang, L., Maekawa, T., Wang, Q., Xiao, W., Liu, Y., Chai, J., Takken, F.L., *et al.* (2012). Structure-function analysis of barley NLR immune receptor MLA10 reveals its cell compartment specific activity in cell death and disease resistance. PLoS Pathog. *8*, e1002752.

Bah, A., and Forman-Kay, J.D. (2016). Modulation of intrinsically disordered protein function by post-translational modifications. J Biol. Chem. 291, 6696-6705.

Bernoux, M., Ve, T., Williams, S., Warren, C., Hatters, D., Valkov, E., Zhang, X., Ellis, J.G., Kobe, B., and Dodds, P.N. (2011). Structural and functional analysis of a plant resistance protein TIR domain reveals interfaces for self-association, signaling, and autoregulation. Cell Host Microbe *9*, 200-211.

Castel, B., Ngou, P.M., Cevik, V., Redkar, A., Kim, D.S., Yang, Y., Ding, P., and Jones, J.D.G. (2019). Diverse NLR immune receptors activate defence via the RPW8-NLR NRG1. New Phytol. 222, 966-980.

Cesari, S., Bernoux, M., Moncuquet, P., Kroj, T., and Dodds, P.N. (2014a). A novel conserved mechanism for plant NLR protein pairs: the "integrated decoy" hypothesis. Front Plant Sci. *5*, 606.

Cesari, S., Kanzaki, H., Fujiwara, T., Bernoux, M., Chalvon, V., Kawano, Y., Shimamoto, K., Dodds, P., Terauchi, R., and Kroj, T. (2014b). The NB-LRR proteins RGA4 and RGA5 interact functionally and physically to confer disease resistance. EMBO J *33*, 1941-1959.

Cesari, S., Moore, J., Chen, C., Webb, D., Periyannan, S., Mago, R., Bernoux, M., Lagudah, E.S., and Dodds, P.N. (2016). Cytosolic activation of cell death and stem rust resistance by cereal MLA-family CC-NLR proteins. Proc. Natl. Acad. Sci. USA *113*, 10204-10209.

Clough, S.J., and Bent, A.F. (1998). Floral dip: a simplified method for Agrobacterium-mediated transformation of Arabidopsis thaliana. Plant J 16, 735-743.

Collins, M.O., Yu, L., Campuzano, I., Grant, S.G., and Choudhary, J.S. (2008). Phosphoproteomic analysis of the mouse brain cytosol reveals a predominance of protein phosphorylation in regions of intrinsic sequence disorder. Mol. Cell Proteomics 7, 1331-1348.

Couto, D., and Zipfel, C. (2016). Regulation of pattern recognition receptor signalling in plants. Nat. Rev. Immunol. *16*, 537-552.

Deslandes, L., Olivier, J., Theulieres, F., Hirsch, J., Feng, D.X., Bittner-Eddy, P., Beynon, J., and Marco, Y. (2002). Resistance to Ralstonia solanacearum in Arabidopsis thaliana is conferred by the recessive RRS1-R gene, a member of a novel family of resistance genes. Proc. Natl. Acad. Sci. USA *99*, 2404-2409.

Holsters, M., Silva, B., Van Vliet, F., Genetello, C., De Block, M., Dhaese, P., Depicker, A., Inze, D., Engler, G., Villarroel, R., et al. (1980). The functional organization of the nopaline A. tumefaciens plasmid pTiC58. Plasmid 3, 212-230.

Horsefield, S., Burdett, H., Zhang, X., Manik, M.K., Shi, Y., Chen, J., Qi, T., Gilley, J., Lai, J.S., Rank, M.X., et al. (2019). NAD(+) cleavage activity by animal and plant TIR domains in cell death pathways. Science *365*, 793-799.

Lazo, G.R., Stein, P.A., and Ludwig, R.A. (1991). A DNA transformation-competent Arabidopsis genomic library in Agrobacterium. Biotechnology (N Y) 9, 963-967.

Huh, S.U., Cevik, V., Ding, P., Duxbury, Z., Ma, Y., Tomlinson, L., Sarris, P.F., and Jones, J.D.G. (2017). Protein-protein interactions in the RPS4/RRS1 immune receptor complex. PLoS Pathog. *13*, e1006376.

Jones, J.D., and Dangl, J.L. (2006). The plant immune system. Nature *444*, 323-329.

Jones, J.D., Vance, R.E., and Dangl, J.L. (2016). Intracellular innate immune surveillance devices in plants and animals. Science *354*.

Krasileva, K.V., Dahlbeck, D., and Staskawicz, B.J. (2010). Activation of an *Arabidopsis* resistance protein is specified by the in planta association of its leucine-rich repeat domain with the cognate oomycete effector. Plant Cell *22*, 2444-2458.

Le Roux, C., Huet, G., Jauneau, A., Camborde, L., Tremousaygue, D., Kraut, A., Zhou, B., Levaillant, M., Adachi, H., Yoshioka, H.*, et al.* (2015). A receptor pair with an integrated decoy converts pathogen disabling of transcription factors to immunity. Cell *161*, 1074-1088.

Lee, D., Bourdais, G., Yu, G., Robatzek, S., and Coaker, G. (2015). Phosphorylation of the plant immune regulator RPM1-INTERACTING PROTEIN4 enhances plant plasma membrane H(+)-ATPase activity and inhibits flagellin-triggered immune responses in Arabidopsis. Plant Cell *27*, 2042-2056.

Lewis, J.D., Lee, A.H., Hassan, J.A., Wan, J., Hurley, B., Jhingree, J.R., Wang, P.W., Lo, T., Youn, J.Y., Guttman, D.S., et al. (2013). The Arabidopsis ZED1 pseudokinase is required for ZAR1-mediated immunity induced by the Pseudomonas syringae type III effector HopZ1a. Proc. Natl. Acad. Sci. USA *110*, 18722-18727.

Ma, K.W., and Ma, W. (2016). YopJ family effectors promote bacterial infection through a unique acetyltransferase activity. Microbiol. Mol. Biol. Rev. *80*, 1011-1027.

Ma, Y., Guo, H., Hu, L., Martinez, P.P., Moschou, P.N., Cevik, V., Ding, P., Duxbury, Z., Sarris, P.F., and Jones, J.D.G. (2018). Distinct modes of derepression of an

Arabidopsis immune receptor complex by two different bacterial effectors. Proc. Natl. Acad. Sci. USA *115*, 10218-10227.

MacLean, B., Tomazela, D.M., Shulman, N., Chambers, M., Finney, G.L., Frewen, B., Kern, R., Tabb, D.L., Liebler, D.C., and MacCoss, M.J. (2010). Skyline: an open source document editor for creating and analyzing targeted proteomics experiments. Bioinformatics 26, 966-968.

Maekawa, T., Kufer, T.A., and Schulze-Lefert, P. (2011). NLR functions in plant and animal immune systems: so far and yet so close. Nat. Immunol. *12*, 817-826.

Meng, F., and Kurgan, L. (2016). DFLpred: High-throughput prediction of disordered flexible linker regions in protein sequences. Bioinformatics *32*, i341-i350.

Mithoe, S.C., and Menke, F.L. (2018). Regulation of pattern recognition receptor signalling by phosphorylation and ubiquitination. Curr. Opin. Plant Bio. *45*, 162-170.

Mittal, R., Peak-Chew, S.Y., and McMahon, H.T. (2006). Acetylation of MEK2 and I kappa B kinase (IKK) activation loop residues by YopJ inhibits signaling. Proc. Natl. Acad. Sci. USA *103*, 18574-18579.

Monteiro, F., and Nishimura, M.T. (2018). Structural, functional, and genomic diversity of plant NLR proteins: an evolved resource for rational engineering of plant immunity. Annu. Rev. Phytopathol. *56*, 243-267.

Mukherjee, S., Keitany, G., Li, Y., Wang, Y., Ball, H.L., Goldsmith, E.J., and Orth, K. (2006). Yersinia YopJ acetylates and inhibits kinase activation by blocking phosphorylation. Science *312*, 1211-1214.

Noutoshi, Y., Ito, T., Seki, M., Nakashita, H., Yoshida, S., Marco, Y., Shirasu, K., and Shinozaki, K. (2005). A single amino acid insertion in the WRKY domain of the *Arabidopsis* TIR-NBS-LRR-WRKY-type disease resistance protein SLH1 (sensitive to low humidity 1) causes activation of defense responses and hypersensitive cell death. Plant J *43*, 873-888.

Park, Y.H., Wood, G., Kastner, D.L., and Chae, J.J. (2016). Pyrin inflammasome activation and RhoA signaling in the autoinflammatory diseases FMF and HIDS. Nature immunology *17*, 914-921.

Peart, J.R., Mestre, P., Lu, R., Malcuit, I., and Baulcombe, D.C. (2005). NRG1, a CC-NB-LRR protein, together with N, a TIR-NB-LRR protein, mediates resistance against tobacco mosaic virus. Curr. Biol. *15*, 968-973.

Sarris, P.F., Duxbury, Z., Huh, S.U., Ma, Y., Segonzac, C., Sklenar, J., Derbyshire, P., Cevik, V., Rallapalli, G., Saucet, S.B.*, et al.* (2015). A plant immune receptor detects pathogen effectors that target WRKY transcription factors. Cell *161*, 1089-1100.

Schreiber, K.J., Bentham, A., Williams, S.J., Kobe, B., and Staskawicz, B.J. (2016). Multiple Domain Associations within the Arabidopsis Immune Receptor RPP1 Regulate the Activation of Programmed Cell Death. PLoS Pathog. *12*, e1005769.

Sohn, K.H., Segonzac, C., Rallapalli, G., Sarris, P.F., Woo, J.Y., Williams, S.J., Newman, T.E., Paek, K.H., Kobe, B., and Jones, J.D. (2014). The nuclear immune receptor RPS4 is required for RRS1SLH1-dependent constitutive defense activation in Arabidopsis thaliana. PLoS Genet. *10*, e1004655.

Takken, F.L., and Tameling, W.I. (2009). To nibble at plant resistance proteins. Science *324*, 744-746.

Tyanova, S., Cox, J., Olsen, J., Mann, M., and Frishman, D. (2013). Phosphorylation variation during the cell cycle scales with structural propensities of proteins. PLoS Comput. Biol. 9, e1002842.

van der Hoorn, R.A., and Kamoun, S. (2008). From Guard to Decoy: a new model for perception of plant pathogen effectors. Plant Cell *20*, 2009-2017.

van der Lee, R., Buljan, M., Lang, B., Weatheritt, R.J., Daughdrill, G.W., Dunker, A.K., Fuxreiter, M., Gough, J., Gsponer, J., Jones, D.T., et al. (2014). Classification of intrinsically disordered regions and proteins. Chem. Rev. 114, 6589-6631.

Wang, J., Hu, M., Wang, J., Qi, J., Han, Z., Wang, G., Qi, Y., Wang, H.-W., Zhou, J.-M., and Chai, J. (2019a). Reconstitution and structure of a plant NLR resistosome conferring immunity. Science *364*, eaav5870.

Wang, J., Wang, J., Hu, M., Wu, S., Qi, J., Wang, G., Han, Z., Qi, Y., Gao, N., Wang, H.-W.*, et al.* (2019b). Ligand-triggered allosteric ADP release primes a plant NLR complex. Science *364*, eaav5868.

Wan, L., Essuman, K., Anderson, R.G., Sasaki, Y., Monteiro, F., Chung, E.H., Osborne Nishimura, E., DiAntonio, A., Milbrandt, J., Dangl, J.L., et al. (2019). TIR domains of plant immune receptors are NAD(+)-cleaving enzymes that promote cell death. Science *365*, 799-803.

Wessling, R., Epple, P., Altmann, S., He, Y., Yang, L., Henz, S.R., McDonald, N., Wiley, K., Bader, K.C., Glasser, C.*, et al.* (2014). Convergent targeting of a common host protein-network by pathogen effectors from three kingdoms of life. Cell Host Microbe *16*, 364-375.

Williams, S.J., Sohn, K.H., Wan, L., Bernoux, M., Sarris, P.F., Segonzac, C., Ve, T., Ma, Y., Saucet, S.B., Ericsson, D.J.*, et al.* (2014). Structural basis for assembly and function of a heterodimeric plant immune receptor. Science *344*, 299-303.

Wu, C.H., Abd-El-Haliem, A., Bozkurt, T.O., Belhaj, K., Terauchi, R., Vossen, J.H., and Kamoun, S. (2017). NLR network mediates immunity to diverse plant pathogens. Proc. Natl. Acad. Sci. USA *114*, 8113-8118.

Yuan, B., Zhai, C., Wang, W., Zeng, X., Xu, X., Hu, H., Lin, F., Wang, L., and Pan, Q. (2011). The Pik-p resistance to Magnaporthe oryzae in rice is mediated by a pair of closely linked CC-NBS-LRR genes. Theor. Appl. Genet. *122*, 1017-1028.

Zhang, X., Bernoux, M., Bentham, A.R., Newman, T.E., Ve, T., Casey, L.W., Raaymakers, T.M., Hu, J., Croll, T.I., Schreiber, K.J.*, et al.* (2017a). Multiple functional self-association interfaces in plant TIR domains. Proc. Natl. Acad. Sci. USA *114*, E2046-E2052.

Zhang, X., Dodds, P.N., and Bernoux, M. (2017b). What do we know about NOD-Like receptors in plant immunity? Annu. Rev. Phytopathol. *55*, 205-229.

STAR★METHODS

KEY RESOURCES TABLE

REAGENT or RESOURCE	SOURCE	IDENTIFIER
ANTIBODIES		
Rabbit polyclonal anti-mCherry antibody	Abcam	Cat.#ab167453; RRID:AB_2571870
Mouse monoclonal anti-GFP antibody, HRP conjugated	Santa Cruz	Cat.#sc-9996 RRID:AB_627695
Mouse monoclonal anti-FLAG antibody, HRP conjugated	Sigma	Cat.# A8592 RRID:AB_439702
Anti-Rabbit IgG HRP secondary antibody in goat	Sigma	Cat.# A0545 RRID:AB_257896
Mouse anti-Phosphoserine antibody	Sigma	Cat.# P3430 RRID:AB_477336
Anti-acetyl lysine antibody	Cell Signaling Technology	Cat.#9441 RRID:AB_331805
BACTERIAL AND VIRUS STRAINS		
Agrobacterium tumefaciens GV3101	Holsters et al. (1980)	N/A
Agrobacterium tumefaciens Agl1	Lazo et al. (1991)	N/A
E.coli DH10b	Invitrogen	Cat.#18290-015
Pst DC3000*(PopP2)*	Williams et al. (2014)	
Pst DC3000*(C321A)*	Williams et al. (2014)	
P. fluorescens (PopP2)	Williams et al. (2014)	
CHEMICALS, PEPTIDES, and RECOMBINANT PROTEINS		
Anti-Flag M2 Beads (affinity gel)	Sigma	Cat.# A2220
GFP-Trap®_A agarose beads	Chromotek	Cat.# gta-20
Anti-protease tablet, complete EDTA-free	Roche	Cat.# 05056489001
Nonidet P-40 Substitute	Roche	Roche-11754599001
PVPP (Polyvinylpolypyrrolidone)	Sigma-Aldrich	Cat.# 77627
SuperSignal West Pico	ThermoFisher	Cat.# 34096
SuperSignal West Femto	ThermoFisher	Cat.# 34580
Prestained Protein Ladder	ThermoFisher	Cat.# 26616
Lambda Protein Phosphatase (Lambda PP)	NEB	Cat.#P0753S
Phosphatase Inhibitor Cocktail 2	Sigma	Cat.#P5726
Phosphatase Inhibitor Cocktail 3	Sigma	Cat.#P0044
CRITICAL COMMERCIAL ASSAYS		
pCR8/GW/TOPO	ThermoFisher	Cat.# K2500-20
EXPERIMENTAL MODELS: ORGANISMS/STRAINS		
Nicotiana tabacum (cultivar 'Petite Gerard')	Sarris et al.(2015)	N/A
Nicotiana benthamiana (Nb)	Sarris et al.(2015)	N/A
Arabidopsis:pAt2:gRRS1-R-HF:pAt3:gRPS4-HA	This paper	N/A
Arabidopsis:pAt2:gRRS1-R$^{1/3/4A}$-HF:pAt3:gRPS4-HA	This paper	N/A
Arabidopsis:pAt2:gRRS1-R^{2A}-HF:pAt3:gRPS4-HA	This paper	N/A
Arabidopsis:pAt2:gRRS1-R$^{1/2/3/4A}$-HF:pAt3:gRPS4-HA	This paper	N/A
Arabidopsis:35S:D56-R-HF	This paper	N/A
Arabidopsis:35S:D56-S-HF	This paper	N/A
OLIGONUCLEOTIDES		

Primers for plasmid construction see **Table S2**.	SIGMA	Custom order
RECOMBINANT DNA		
pICSL86977	TSL SynBio	Addgene#86180
pICSL86922	TSL SynBio	N/A
pICSL01005	TSL SynBio	N/A
pICSL01003	TSL SynBio	N/A
pICSL86900	TSL SynBio	Addgene#86178
pICSL47732	TSL SynBio	AddGene #48000
pICSL47742	TSL SynBio	AddGene #48001
pICH86988	Sarris et al.(2015)	Addgene#48076
pK7WGF2-35S-GFP	This paper	N/A
pICSL86977-35S-TIR^{RRS1}-GFP	This paper	N/A
pICSL86977-35S-D56-R-HF	Ma et al., 2018	N/A
pICSL86977-35S-D56-S-HF	Ma et al., 2018	N/A
pICH86988-35S-AvrRps4-mCherry	Ma et al., 2018	N/A
pICH47751-35S-AvrRps4(E175A/E187A)-mCherry	Ma et al., 2018	N/A
pICSL86977-35S-mCherry	Ma et al., 2018	N/A
pICSL86977-35S-PopP2-mCherry	Ma et al., 2018	N/A
pICSL86977-35S-PopP2(C321A)-mCherry	Ma et al., 2018	N/A
pICSL86977-35S-RRS1-R-HF	Ma et al., 2018	N/A
pICSL86977-35S-RRS1-R^{1A}-HF	This paper	N/A
pICSL86977-35S-RRS1-R^{3A}-HF	This paper	N/A
pICSL86977-35S-RRS1-R^{4A}-HF	This paper	N/A
pICH86988-35S-RRS1-S-HF	Sarris et al.(2015)	N/A
pICSL86977-35S-RRS1-R^{2A}-HF	This paper	N/A
pICSL86977-35S-RRS1-R$^{1/3/4A}$-HF	This paper	N/A
pICSL86977-35S-RRS1-R$^{1/2/3/4A}$-HF	This paper	N/A
pICSL86977-35S-RRS1-R^{slh1}1/3/4A-HF	This paper	N/A
pICSL86977-35S-RRS1-R$^{K1221Q/1/3/4A}$-HF	This paper	N/A
pICSL86977-35S-RRS1-R^{1D}-HF	This paper	N/A
pICSL86977-35S-RRS1-R^{3D}-HF	This paper	N/A
pICSL86977-35S-RRS1-R^{4D}-HF	This paper	N/A
pICSL86977-35S-RRS1-R$^{1/3/4D}$-HF	This paper	N/A
pICSL86977-35S-RRS1-R^{2D}-HF	This paper	N/A
pICSL86977-35S-RRS1-S(T1212A)-HF	This paper	N/A
pICSL86977-35S-RRS1-S(T1212D)-HF	This paper	N/A
pICSL86977-35S-RRS1-R(T1214D/K1221Q)-HF	This paper	N/A
pICSL86977-35S-RRS1-R(T1214A/K1221R)-HF	This paper	N/A
pICSL86900-35S-cCFP-RRS1-R-nVenus	This paper	N/A
pICSL86900-35S-cCFP-RRS1-S-nVenus	This paper	N/A
pICSL86977-35S-D56-R^{1A}-HF	This paper	N/A
pICSL86977-35S-D56-R^{3A}-HF	This paper	N/A
pICSL86977-35S-D56-R^{4A}-HF	This paper	N/A
pICSL86977-35S-D56-R^{2A}-HF	This paper	N/A
pICSL86977-35S-D56-R$^{1/3/4A}$-HF	This paper	N/A
pICSL86977-35S-D56-R$^{1/2/3/4A}$-HF	This paper	N/A
pICSL86977-35S-D56-R$^{1/3/4D}$-HF	This paper	N/A
pICSL4723-pAt2:gRRS1-R-HF:pAt3:gRPS4-HA	This paper	N/A
pICSL4723-pAt2:gRRS1-R$^{1/3/4A}$-HF:pAt3:gRPS4-HA	This paper	N/A
pICSL4723-pAt2:gRRS1-R^{2A}-HF:pAt3:gRPS4-HA	This paper	N/A
pICSL4723-pAt2:gRRS1-R$^{1/2/3/4A}$-HF:pAt3:gRPS4-HA	This paper	N/A
pICSL47732-CSVMV:cyPET	This paper	N/A

pICSL47761-pUbi10:nYFP-RRS1-R-HF	This paper	N/A
pICSL47761-pUbi10:nYFP-RRS1-S-HF	This paper	N/A
pICSL47761-pUbi10:nYFP-RRS1-$R^{1/3/4A}$-HF	This paper	N/A
pICSL47751-35S:cYFP-RPS4-HF	This paper	N/A
SOFTWARE AND ALGORITHMS		
Scaffold	Proteome Software Inc	N/A
Skyline	MacLean et al., 2010	N/A
ImageJ	NIH	ver 1.49a; RRID:SCR_003070
R	On-line	https://www.r-project.org/

LEAD CONTACT AND MATERIALS AVAILABILITY

Further information and requests for resources and reagents should be directed to and will be fulfilled by the Lead Contact, Jonathan Jones (jonathan.jones@tsl.ac.uk)

EXPERIMENTAL MODEL AND SUBJECT DETAILS

Arabidopsis

Arabidopsis plants were grown in short days (10 hr light/14 hr dark) at 21°C or 28°C (for RRS1-R^{T1214A} autoimmune plants). For generation of stable transgenic *Arabidopsis*, standard floral dip transformation method was used (Clough and Bent, 1998).

Nicotiana benthamiana

Nicotiana benthamiana (*Nb*) and *Nicotiana tabacum* (cultivar 'Petite Gerard') plants were sown on soil and grown at 24°C under long-day photoperiod (16 hr light/8 hr dark) with 55% relative humidity. Leaves of 4 to 5 week-old plants were used for *Agrobacterium tumefaciens*-mediated transient expression for Immunoblotting, HR, BiFC or co-IP assays.

Bacterial Strains

P. syringae pv. tomato DC3000(PopP2) and *P. syringae pv. tomato* DC3000(C321A) were cultured in King's B liquid media containing rifampicin (50 µg/mL) and gentamycin (20 µg/mL) overnight. Pf0-1 (T3SS) carrying the PopP2 strains were grown on King's B plate supplemented with antibiotics (Chloramphenicol 30 µg/ml, Tetracycline 5 µg/ml and gentamicin 20 µg/ml) at

28°C overnight. Bacterial cells were collected by centrifugation and resuspended in infiltration buffer (10 mM $MgCl_2$, pH 5.6).

METHOD DETAILS

Plasmid Construction

All the Golden Gate compatible epitope tags including C-terminal GFP/mCherry and N- or C-terminal cCFP and nVenus tags for multi-color BiFC, HF-tagged D56-R/S, mcherry-tagged wild-type and mutant variants of AvrRps4 and PopP2 used in this study were described previously (Ma et al., 2018). The C-terminally GFP-tagged TIR^{RRS1}, cCFP-RRS1-S-nVenus and cCFP-RRS1-R-nVenus constructs were generated using the Golden Gate assembly cloning procedure described previously (Ma et al., 2018). Phosphorylation mutations of RRS1-R were generated using Goldern Gate cloning with primers containing *BbsI* site and the introduced mutations. The multiple mutation was achieved by successive mutagenesis steps. All final constructs used in this study were validated by DNA sequencing.

Agrobacterium-Mediated Tobacco Transient Assays (HR)

Agrobacterium. tumefaciens strain GV3101 harbouring indicated binary constructs were streaked on selective L-medium agar plates and grown for 24-48 h. Cultures were grown in liquid L-medium overnight in a shaking incubator (200 rpm, 28°C). Cells were harvested by centrifugation and re-suspended in infiltration medium (10mM $MgCl_2$, 10mM MES, pH 5.6). For co-expression, each bacterial suspension carrying individual constructs was adjusted to OD_{600}=0.5 ($2.5x10^8$ cfu/mL) in the final mix for infiltration. Leaf sections of 5-week-old *N. tabacum* (tobacco) fully-expanded leaves were infiltrated with 1 ml needleless syringe. HR phenotypes were photographed at 3-4 dpi.

HR assay in *Arabidopsis*

For infiltration into *Arabidopsis* leaves, PopP2 was delivered using the *Pseudomonas fluorescens* Pf0-1 engineered with a type III secretion system

was described previously (Sohn et al., 2014). Briefly, Pf0-1 (T3SS) carrying the PopP2 strains were grown on King's B agar plate supplemented with antibiotics (Chloramphenicol 30 μg/ml, Tetracycline 5 μg/ml or gentamicin 20 μg/ml) at 28°C overnight. Bacteria were harvested and resuspended at OD_{600} of 0.2 in infiltration buffer. Fully expanded leaves of 5-week-old *Arabidopsis* were hand infiltrated with a 1 ml needleless syringe and cell death was assessed at 24 h post-infiltration.

Disease Resistance Assay

For bacterial growth assay, *P. syringae pv. tomato* DC3000(PopP2) and *P. syringae pv. tomato* DC3000(C321A) were grown in King's B liquid media containing rifampicin (50 μg/mL) and gentamycin (20 μg/mL) overnight. Bacteria were harvested, resuspended with infiltration buffer (10 mM $MgCl_2$, pH 5.6) at a concentration of OD_{600}=0.0005 and infiltrated into fully-expanded leaves of 4-5 weeks-old Arabidopsis plants. The infected leaves are harvested at 0 and 3 days post inoculation to quantify bacterial colonies. Statistical significance is indicated by letters ($p < 0.01$, one-way ANOVA followed by Tukey's post hoc test).

Protein Extraction, Immunoprecipitation and Immunoblot Analysis

Protein samples were collected from *Nb* leaves 48 hours post agroinfiltratiion, flash-frozen in liquid nitrogen and stored at -80°C. For protein extraction, frozen samples were ground in liquid nitrogen and the powder was mixed with an equal volume of ice-cold GTEN buffer (10% glycerol, 150 mM Tris-HCl pH 7.5, 1 mM EDTA, 150 mM NaCl) supplemented with 10 mM DTT, 0.2% (vol/vol) Nodinet-40, Anti-protease tablet (Complete EDTA-free Roche) and 2% PVPP (Polyvinylpolypyrrolidone). Homogenisation was achieved by mixing on a rotator for 20 min at 4°C. The lysates were then centrifuged at 5000 g for 30 min at 4°C, and the supernatant was filtered through 0.45 mm filters. The filtered protein extract was mixed with 3xSDS loading buffer (30% glycerol, 3.3% SDS, 94 mM Tris-HCl pH 6.8, 0.05% (vol/vol) bromophenol blue) supplemented with 10 mM DTT for immunoblot analyses as input samples or

for Westerns. Immunoprecipitations were conducted on 1.5 ml of filtered extract incubated with 30 µl Antibodies-coupled agarose beads (Anti-FLAG M2, Sigma; Anti-GFP, Chromotek) for 2 h at 4°C under gentle agitation. After incubation, beads were collected via centrifugation at 7000 rpm for 30 seconds and then washed three times in washing buffer (GTEN buffer supplemented with 10 mM DTT, 0.2% Nodinet-40 and Anti-protease tablet). The bringing protein was released from the beads by re-suspendeding in SDS-loading buffer with 10 mM DTT and denatured by boiling at 95°C for 10 min. The co-immunooprecipated proteins were separated by SDS-PAGE and analysed by immunoblotting. For lambda phosphatase treatment, the beads after immunoprecipitation were incubated with lambda phosphatase (New England Biolabs, P0753) at 37°C for 1h and subsequently subjected to SDS–PAGE. To detect acetylated RRS1, immunoprecipitated RRS1 samples were separated by SDS-PAGE and analysed by immunoblotting using α-acetyl lysine antibody (Cell Signaling, #9441).

Tris-Glycine polyacrylamide (PAA) gels were prepared with 5% polyacrylamide for the stacking gel, and 10 or 12% polyacrylamide for resolving gels in this study. The pre-stained protein ladder (PageRuler, ThermoFisher) was used as molecular weight marker. Proteins were transferred to Immobilon-P PVDF membranes (Merck Millipore), using a semi-dry transfer apparatus supplied by Trans-Blot Turbo (Bio-Rad). After blocking at room temperature for 1 h or overnight at 4 °C in TBST (Tris-Buffered Saline with 0.1% Tween) containing 5% (w/v) non-fat dry milk, membrane was incubated with Horseradish Peroxidate (HRP) conjugated antibodies (Anti-FLAG M2, 1:10000 dilution, Sigma; Anti-GFP, 1:10000 dilution, Santa Cruz Biotechnology) in TBST supplemented with 5% milk by gentle agitation at room temperature for 1 h. The membrane was then washed 3 times with TBST for 5 minutes, and once in TBS (Tris-Buffered Saline). Chemiluminescence detection for proteins of interest was carried out firstly by incubating the membrane with developing reagents

(SuperSignal West Pico & West Femto), and then exposing it to X-ray film (Fuji) or by imaging using ImageQuant LAS 4000 (Life Sciences).

Bimolecular Fluorescence Complementation (BiFC) Assay

BiFC analysis was performed in transient transfection assays as described previously (Ma et al., 2018). Briefly, N-terminal fragment of YFP and C-terminal fragment of YFP were fused to determine proximity of proteins. *A. tumefaciens* strains carrying BiFC constructs and effector protein constructs (or their mutant controls) tagged with mCherry were co-infiltrated with cyPET as expression control. Leaves of 4-week-old *N. benthamiana* plants were agroinfiltrated using a 1 mL needleless syringe. Leaf samples were taken for imaging between 40-60hpi. Each experiment replicated independently at least 3 times.

All microscopic analyses were conducted on live leaf sections with water as imaging medium. Live-cell imaging was observed by a Leica DM6000B/TCS SP5 laser-scanning confocal microscope (Leica microsystems, Bucks, UK), using a 63x water immersion objective with NA=1.2 (Leica PL-APO CS2). The CFP, YFP and RFP fluorophore were excited using sequential scan with 405nm, 488 and 585nm laser diodes and their fluorescence emissions were collected between 420-440nm, 530-550nm and 580-620nm, respectively. Images acquired at laser power of 35% transmittance for 425 nm (HyD1), 35% transmittance for 458 nm (PMT), 15-20% for 561 nm (HyD3); 256 X 256 8-bit pixel format; scan speed 400 Hz; zoom factor 3. Same setting was used for each experiment.

Sample Preparation for Mass Spectrometry

To identify the C-terminus of RRS1-R/S phosphosites, approximately 10 g of 4-week-old transgenic *Arabidopsis* plants overexpressing HF-tagged D56-R/D56-S were ground for total protein extraction using GTEN buffer. To relatively quantify acetylated peptides, plant samples were harvested from *N. benthamiana* leaves 48 hr after *Agrobacterium* infiltration and subsequently homogenized using GTEN buffer. The D56-R/D56-S protein was then enriched by immunoprecipitation using anti-FLAG M2 Affinity Gel (A2220, Sigma-

Aldrich) according to the manufacturer's instructions. The bound protein was eluted with 50 µL 2XSDS–PAGE loading buffer by boiling the beads at 95°C for 5 min and separated in 4-12% NuPAGE gel (Invitrogen). After staining with SimplyBlue™ SafeStain(Invitrogen, LC6060), bands containing the D56-R/D56-S protein were cut from the gel and digested with trypsin, and subject to mass spectrometric analysis.

LC-MS/MS Analysis

LC-MS/MS analysis was performed using a hybrid mass spectrometer Orbitrap Fusion and a nanoflow UHPLC system U3000 (Thermo Scientific). Tryptic peptides, dissolved in 2% Acetonitril, 0.2% Trifluoroacetic acid (TFA), were injected onto a reverse phase trap column nanoEase M/Z Symmetry C18, beads diameter 5µm, 180µm x 20mm (Waters, Corp.). The column was operated at the flowrate 20µl/min in 2% Acetonitril, 0.05% TFA, after 2.5min the trap column was connected to the analytical column nanoEase M/Z HSS C18 T3 Column, beads diameter 1.8µm, 75µm x 250mm (Waters). The column equilibrated with 3%B before the injection in 3%B (A: 0.1% Formic Acid (FA), B: 80% Acetonitrile in 0.05% FA) was subsequently eluted with the following steps of linear gradient: 2.5min 3%B, 5min 6.3%B, 13min 12.5%B, 50min 42.5%B, 58min 50%B, 61min 60%B, 63min 99%B, 66min 99%B, 67min 3%B, 90min 3%B. The flow rate was set to 200 nL*min-1. The mass spectrometer was operated in positive ion mode with nano-electrospray ion source. Molecular ions were generated by applying voltage +2.2kV to a conductive union coupling the column outlet with fussed silica PicoTip emitter, ID 10µm (New Objective, Inc.). The ion transfer capillary temperature was set to 275 ºC and the focusing voltages in the ion optics were in factory default setting.

Acetylated Peptides Quantitative Assay

Peptides quantitative assay was performed using Parallel Reaction Monitoring (PRM) technology on Orbitrap Fusion. Briefly, the method allows to enter a list of masses in m/z, z, retention time format and the MS method

fragments the precursors and acquire MS/MS spectra only. Thus, chromatographical peaks can be integrated if the scan frequency is kept at least 10 scans across the peak. Chromatographical method was the same as above with the exceptions of length of the gradient in steps 12.5%B to 42.5%B over 60min. MS settings were: AGC = 100000, maximum injection time = 22ms, resolution = 15000 and HCD normalized collision energy CE=30.

Software Processing and Peptides Identification

Peak lists in the format of Mascot generic files were prepared from raw data using MS Convert (Proteowizard project) and sent to a peptide search on Mascot server v2.4.1 using Mascot Daemon (Matrix Science, Ltd.). Peak lists were searched against protein databases including typical proteomics contaminants such as keratins, etc. Tryptic peptides with up to 2 possible mis-cleavages and charge states +2, +3, +4 were allowed in the search. The following peptide modifications were included in the search: carbamidomethylated Cysteine (static) and oxidized Methionine, phosphorylated Serine, Threonine, Tyrosine (variable). Data were searched with a monoisotopic precursor and fragment ion mass tolerance 10ppm and 0.6Da respectively. Decoy database was used to validate peptide sequence matches. Mascot results were combined in Scaffold v4.4.0 (Proteome Software Inc.) and exported to Excel (Microsoft) for further processing and comparisons.

In Scaffold, the peptide and protein identifications were accepted if probability of sequence match and protein inference exceeded 95.0% and 99% respectively and at least 2 unique peptides were identified per protein. Protein probabilities were calculated in Scaffold by the Protein Prophet algorithm; proteins that contained similar peptides and could not be differentiated based on MS/MS analysis alone were grouped to satisfy the principles of parsimony (Searle, 2010). Several identified peptides were selected for quantitative analysis with open source software Skyline (MacLean et al., 2010). Calculated peak areas were exported in a text-based format and further interpreted in

Excel program. (Microsoft) Together with aceylted peptides were targeted non modified peptides and used as reporters of protein concentration. These values were used to normalize the peak areas in independent replicates.

Quantification and Statistical Analysis

For immunoblotting quantification, the relative intensities of immunoblotting band were processed and quantified with Image J software (National Institutes of Health). For BiFC assay, image analyses and signal intensity quantifications were performed with FIJI 2.0.0 (http://fiji.sc/Fiji). Box-whisker plots were drawn for quantification analysis, and each data point indicates the YFP intensity normalized to cyPET intensity in individual single cells. Each biological replicate was indicated in different colors. Biological significance of the comparison of means was determined by one-way ANOVA for multiple pairwise comparisons, followed by post hoc TukeyHSD analysis. Significance is indicated in the figures with same letter if $P<0.05$. P-values for all pairwise comparisons are summarized in Table S3.

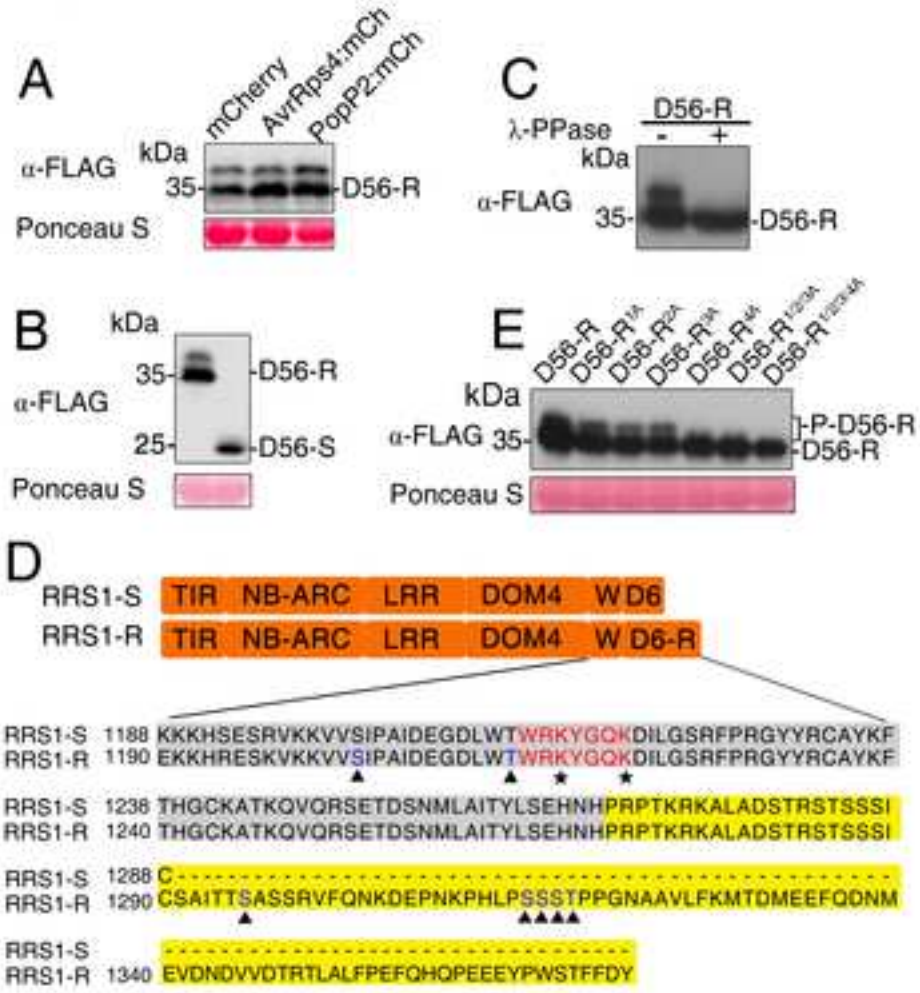

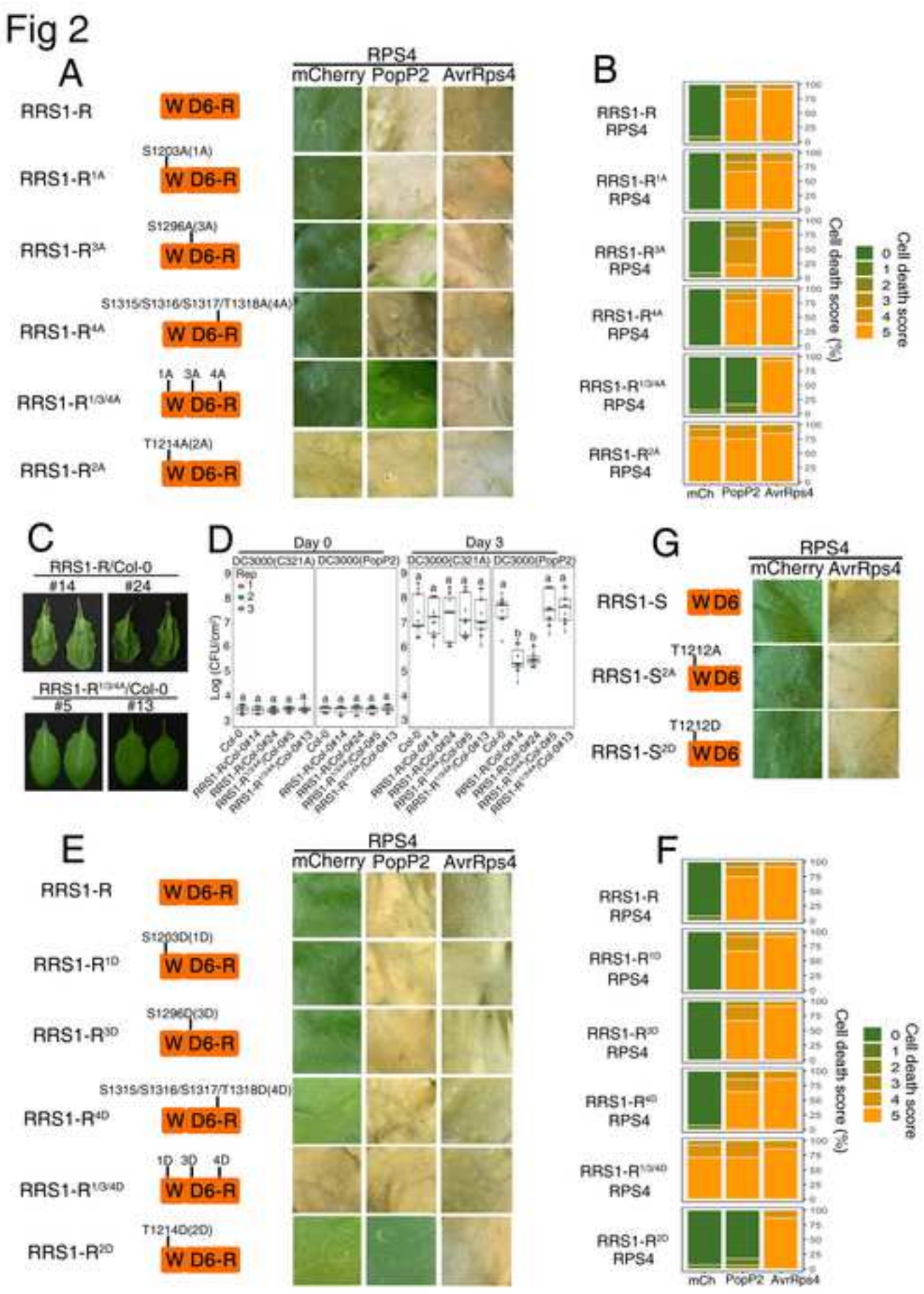

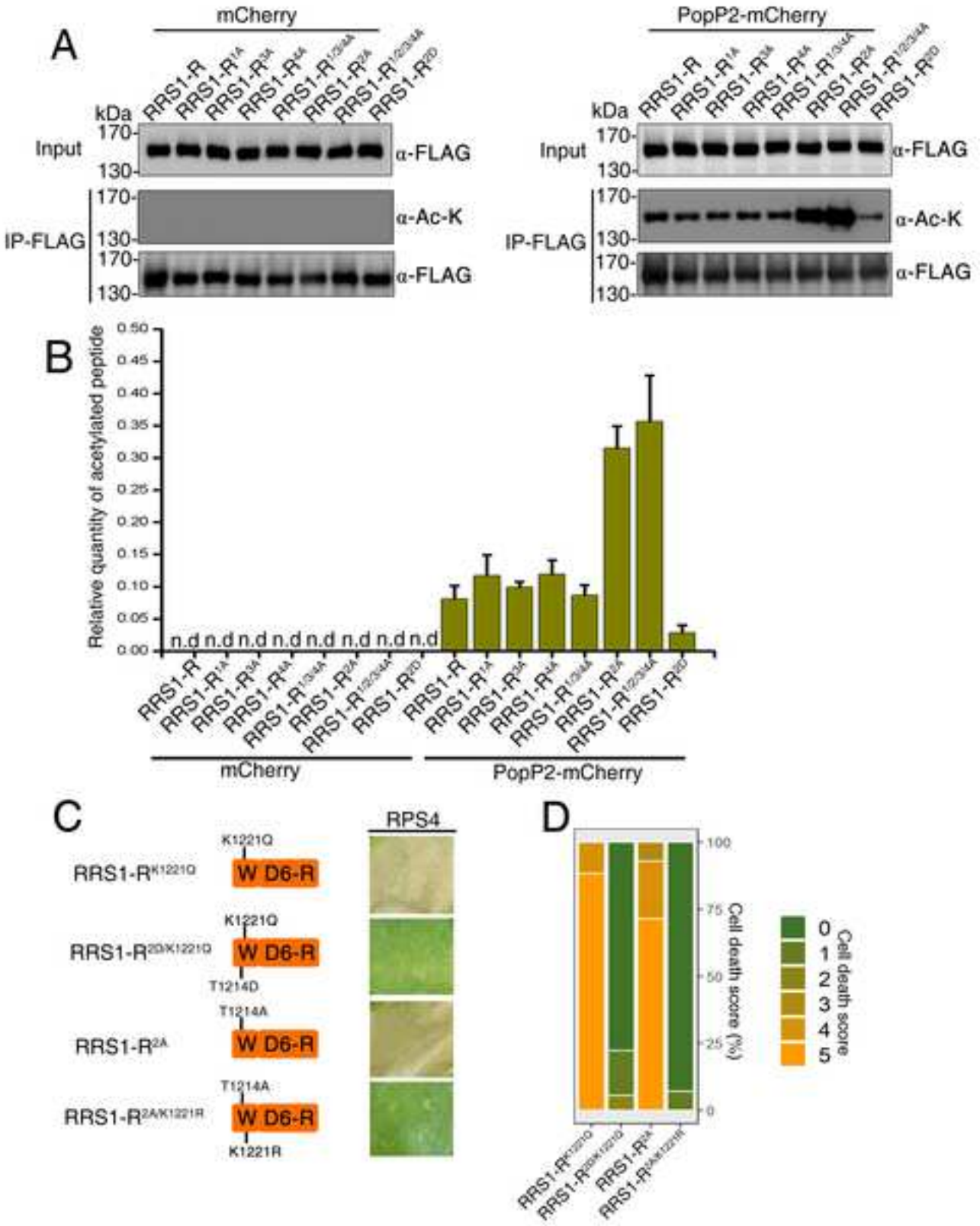

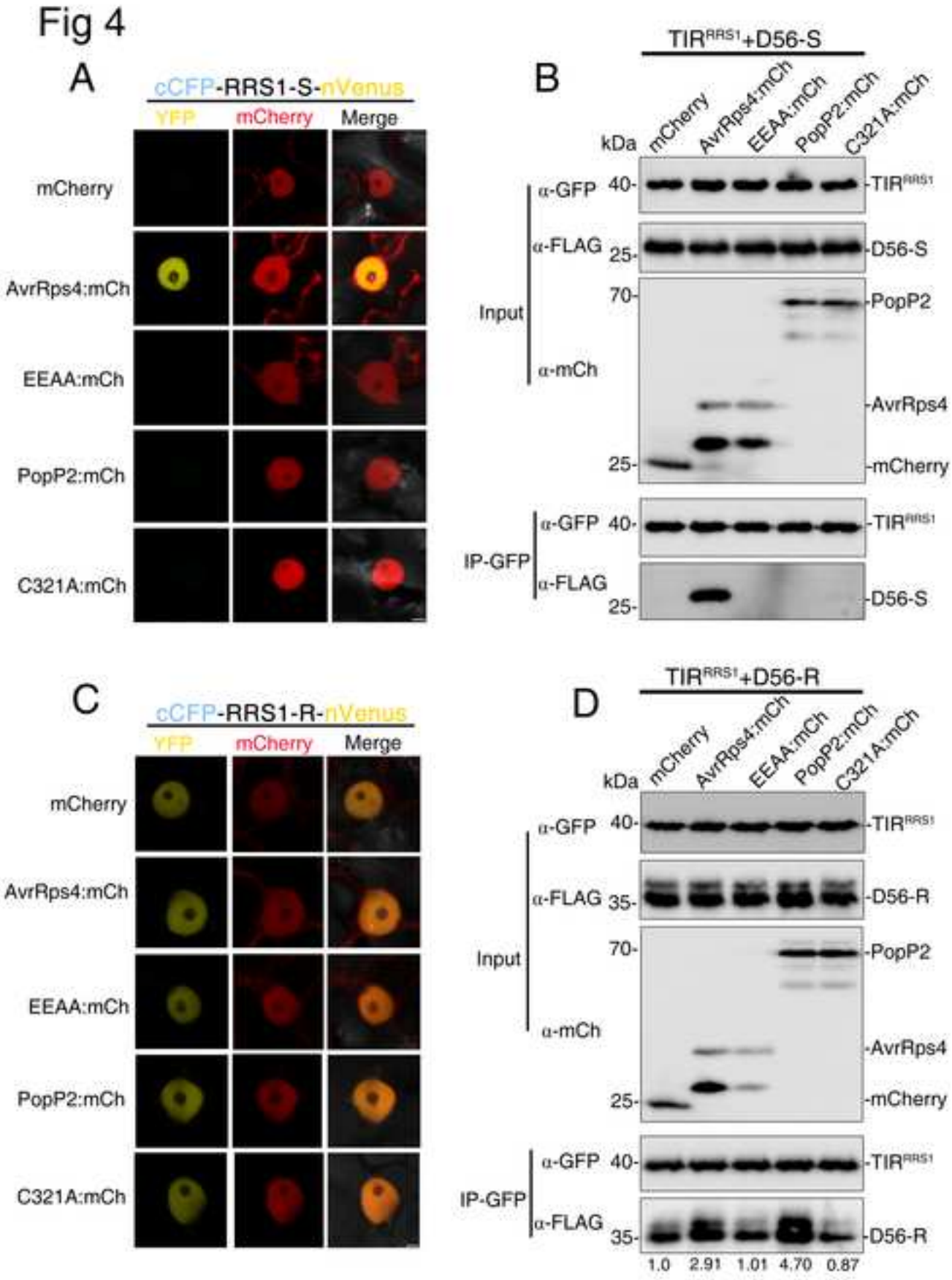

Fig 5

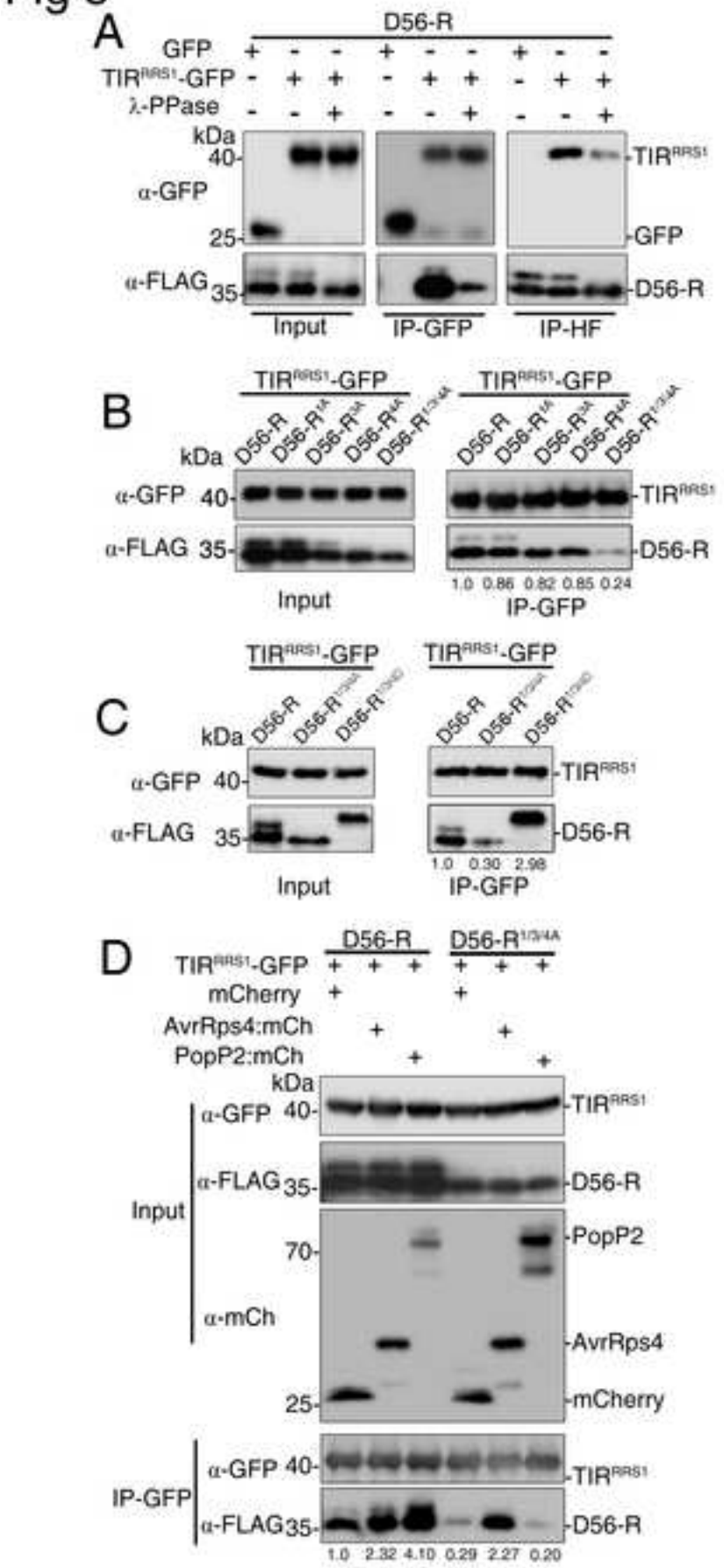

Fig 6

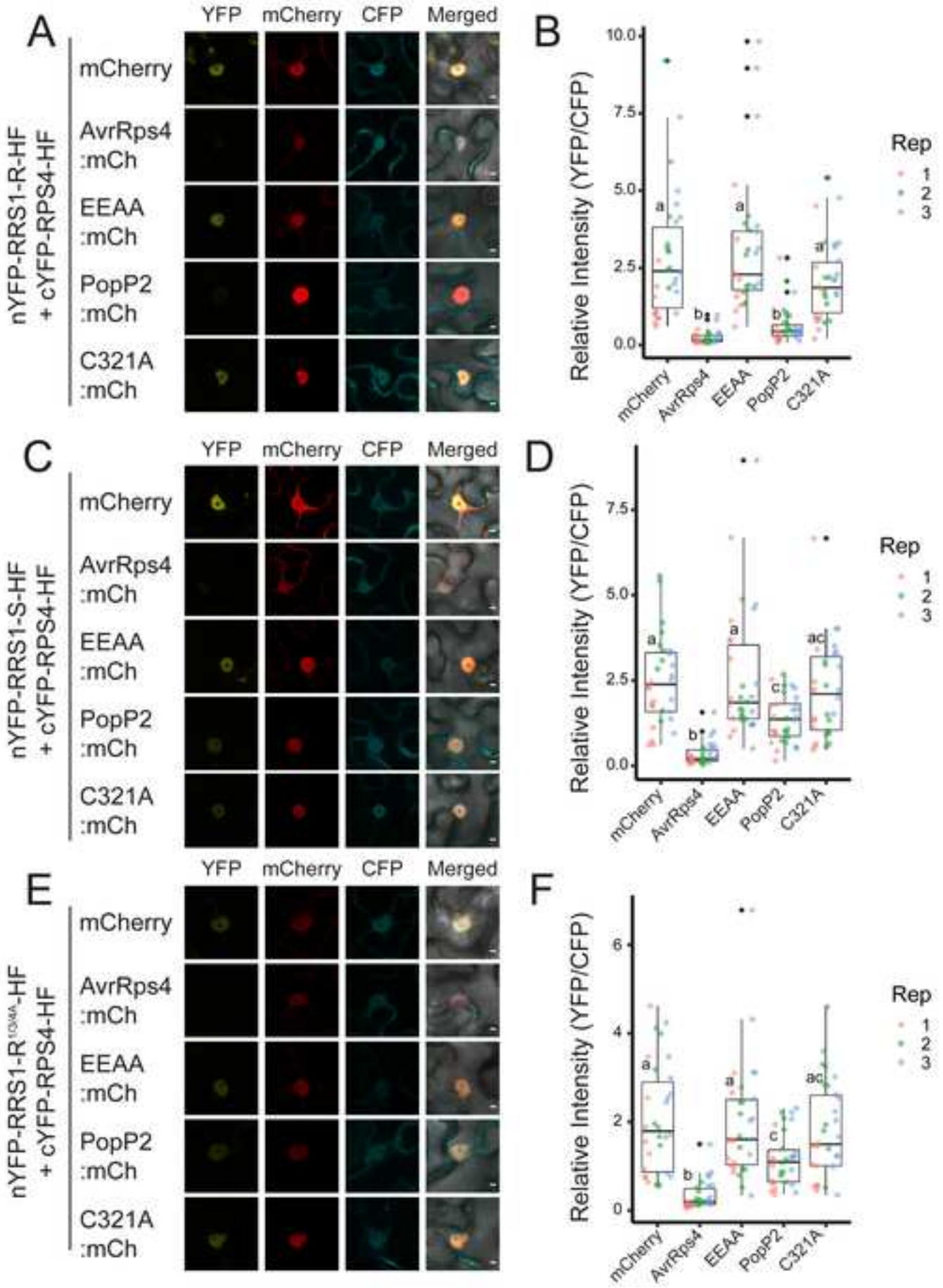

Click here to access/download

Supplemental Videos and Spreadsheets

Supplementary Table S1, 2 and 3_Final.pdf